

Prepared in cooperation with the National Park Service

# Simulation of Deep Ventilation in Crater Lake, Oregon, 1951–2099



Scientific Investigations Report 2016–5046

**U.S. Department of the Interior**  
**U.S. Geological Survey**

**Cover:** Photograph of Crater Lake, Oregon, looking southeast across the lake.  
Photograph by National Park Service, undated.

# **Simulation of Deep Ventilation in Crater Lake, Oregon, 1951–2099**

By Tamara M. Wood, Susan A. Wherry, Sebastiano Piccolroaz, and Scott F. Girdner

Prepared in cooperation with the National Park Service

Scientific Investigations Report 2016–5046

**U.S. Department of the Interior**  
**U.S. Geological Survey**

**U.S. Department of the Interior**  
SALLY JEWELL, Secretary

**U.S. Geological Survey**  
Suzette M. Kimball, Director

U.S. Geological Survey, Reston, Virginia: 2016

For more information on the USGS—the Federal source for science about the Earth, its natural and living resources, natural hazards, and the environment—visit <http://www.usgs.gov> or call 1–888–ASK–USGS.

For an overview of USGS information products, including maps, imagery, and publications, visit <http://store.usgs.gov>.

Any use of trade, firm, or product names is for descriptive purposes only and does not imply endorsement by the U.S. Government.

Although this information product, for the most part, is in the public domain, it also may contain copyrighted materials as noted in the text. Permission to reproduce copyrighted items must be secured from the copyright owner.

Suggested citation:

Wood, T.M., Wherry, S.A., Piccolroaz, S., and Girdner, S.F., 2016, Simulation of deep ventilation in Crater Lake, Oregon, 1951–2099: U.S. Geological Survey Scientific Investigations Report 2016–5046, 43 p., <http://dx.doi.org/10.3133/sir20165046>.

ISSN 2328-0328 (online)

# Contents

Abstract.....	1
Introduction.....	1
Purpose and Scope .....	3
Methods.....	3
Datasets.....	3
Historical Water Quality and Meteorological Data .....	3
Climate Data.....	4
Models .....	4
Data Processing.....	6
Historical Water-Quality and Meteorological Data for the 1-Dimensional Deep Ventilation Model .....	6
Historical Water-Quality and Meteorological Data for the Dynamic Reservoir Simulation Model .....	7
Future Climate Data .....	7
Air and Lake Surface Temperature.....	7
Wind Speed .....	11
One-Dimensional Lake Temperature Modeling.....	13
One-Dimensional Deep Ventilation Model .....	13
Initial Values of Calibration Parameters .....	13
Reference Diffusivity Profile .....	14
Calibration.....	16
Dynamic Reservoir Simulation Model.....	23
Calibration.....	23
One-Dimensional Deep Ventilation Model Validation.....	26
Results of Future Climate Scenarios .....	28
Comparisons to Future-Climate Studies of Other Lakes .....	37
Conclusions.....	39
Summary.....	40
Acknowledgments .....	41
References Cited.....	41

## Figures

1. Map showing sampling site and climate model grid, Crater Lake, Oregon .....	2
2. Flow chart showing approach used to convert wind stress to water column mixing in the 1-dimensional deep ventilation model and the DYNamic REservoir Simulation Model.....	5
3. Time series of December-to-May averages of air temperature and water temperature at 20 meter depth, and water temperature at 20 meter depth simulated by the lumped model <i>air2water</i> , during the calibration period 1993–2011 at Crater Lake, Oregon .....	9
4. Time series of December-to-May averages of downscaled air temperature from general circulation models, and water temperature at 20 meter depth as determined with the <i>air2water</i> model, through baseline (1951–2005) and future climate (2006–2099) conditions at Crater Lake, Oregon .....	10

## Figures—Continued

5. Graphs showing cumulative distribution functions of measured and simulated daily wind speed for the common historical period 1991–2005, and the original and adjusted minimum, mean, and maximum wind speed from three general circulation models and two representative concentration pathways during baseline (1951–2005) and future (2006–2099) conditions at Crater Lake, Oregon .....12
6. Graph showing ten salinity profiles at Site B, Crater Lake, Oregon, collected between July and September, 1991–1998, and a 4th order polynomial fit to the average of the profiles .....14
7. Graph showing reference turbulent diffusivity profile for the 1-dimensional deep ventilation model of Crater Lake, Oregon .....16
8. Contour plot showing measured temperature data, Crater Lake, Oregon, 2000–2006 .....18
9. Contour plot showing temperature simulated with the 1-dimensional deep ventilation model, Crater Lake, Oregon, 2000–2006 .....18
10. Graphs showing comparison of selected measured temperature profiles with profiles simulated with the 1-dimensional deep ventilation model, Crater Lake, Oregon, 2003–2005 .....19
11. Graphs showing comparison of measured temperature to temperature simulated with the 1-dimensional deep ventilation model at depths between 20 and 530 meters, Crater Lake, Oregon, 2000–2006 .....20
12. Graphs showing temperature and diffusivity profiles over the autumn to spring months of 2002–2003, when no deep ventilation of the water column occurred, Crater Lake, Oregon .....21
13. Graphs showing temperature and diffusivity profiles over the autumn to spring months of 2003–2004, when deep ventilation of the water column occurred, Crater Lake, Oregon .....21
14. Graphs showing upper and lower water-column heat content calculated from thermistors and from temperatures simulated by the 1-dimensional deep ventilation model of Crater Lake, Oregon, during the calibration years 2000–2006 and the validation years 1994–1999 and 2008–2011 .....22
15. Graphs showing comparison of selected measured temperature profiles to profiles simulated with the DYnamic REservoir Simulation Model, Crater Lake, Oregon, 2001–2003 .....25
16. Graphs showing comparison of measured temperature to temperature simulated with the DYnamic REservoir Simulation Model, Crater Lake, Oregon, 1999–2007 .....26
17. Graphs showing upper and lower water-column heat content calculated from thermistors and from temperatures simulated by the DYnamic REservoir Simulation Model of Crater Lake, Oregon, 1999–2007 .....27
18. Scatterplot showing comparison of the change in heat content between December and June as calculated from thermistor data and as simulated with the 1-dimensional deep ventilation model of Crater Lake, Oregon, 1994–1999, 2000–2006, and 2008–2010 .....28
19. Contour plots showing temperature of Crater Lake, Oregon, simulated with the 1-dimensional deep ventilation model, for baseline and future conditions from three general circulation models and two representative concentration pathways .....30

## Figures—Continued

20. Graphs showing surface and bottom temperatures of Crater Lake, Oregon, simulated with the 1-dimensional deep ventilation model, for baseline and future conditions from three general circulation models and two representative concentration pathways.....33
21. Time series showing heat content in Crater Lake, Oregon, as calculated from temperatures simulated by the 1-dimensional deep ventilation model for baseline and future conditions from three general circulation models and two representative concentration pathways .....36

## Tables

1. Statistical characteristics of air temperature and water temperature for the historical period of record and for the baseline and future conditions periods from three general circulation models (GCMs) and two representative concentration pathways.....9
2. Statistical characteristics of wind speed for the historical period of record and for the baseline and future conditions periods from three general circulation models (GCMs) and two representative concentration pathways .....13
3. Rate of change in heat content in the deep and mid water column, and the calculated hydrothermal flux between July and September, Crater Lake, Oregon, 1990–2013 .....15
4. Calibration parameters for the 1-dimensional deep ventilation model of Crater Lake, Oregon.....17
5. Goodness-of-fit statistics at thermistor target depths for temperature simulated with the 1-dimensional deep ventilation model, Crater Lake, Oregon, 2000–2006 .....17
6. Goodness-of-fit statistics for heat content calculated from temperatures simulated by the 1-dimensional deep ventilation model of Crater Lake, Oregon, 1994–2011 .....22
7. DYnamic REservoir Simulation Model default parameter values .....24
8. Goodness of fit statistics for the DYnamic REservoir Simulation Model of Crater Lake, Oregon, 1999–2007 .....24
9. Change in heat content from December to June in the lower water column of Crater Lake, Oregon, 1994–2011 .....27
10. Linear regression models of upper and lower water-column heat content in Crater Lake, as calculated from temperatures simulated by the 1-dimensional deep ventilation model, for baseline and future conditions from three general circulation models and two representative concentration pathways.....29
11. Frequency of deep ventilation during the historical measurement period and during the baseline and future conditions periods from three general circulation models and two representative concentration pathways, Crater Lake, Oregon.....35
12. Replacement volume and residence time in the deep lake, determined during baseline conditions (1951–2005) and future conditions (2045–2099) from three general circulation models and two representative concentration pathways at Crater Lake, Oregon .....35
13. Long-term changes in lower water-column temperature in deep lakes (> 100 m depth), based on historical measurements and modeling studies of future climate scenarios.....38

## Conversion Factors

Inch/Pound to International System of Units

<b>Multiply</b>	<b>By</b>	<b>To obtain</b>
Length		
kilometer (km)	0.6214	mile (mi)
meter (m)	3.281	foot (ft)
Area		
square meter (m <sup>2</sup> )	10.76	square foot (ft <sup>2</sup> )
Volume		
cubic kilometer (km <sup>3</sup> )	0.2399	cubic mile (mi <sup>3</sup> )
Flow rate		
cubic meter per day (m <sup>3</sup> /d)	35.31	cubic foot per day (ft <sup>3</sup> /d)
Mass		
kilogram (kg)	2.205	pound avoirdupois (lb)
Density		
kilogram per cubic meter (kg/m <sup>3</sup> )	0.06242	pound per cubic foot (lb/ft <sup>3</sup> )
Heat Energy		
joule (J)	0.2391	calorie (cal)
Heat Flux		
Watt per square meter (W/m <sup>2</sup> )	79.96	calorie per hour per square foot [(cal/h)/ft <sup>2</sup> ]

Temperature in degrees Celsius (°C) may be converted to degrees Fahrenheit (°F) as

$$^{\circ}\text{F} = (1.8 \times ^{\circ}\text{C}) + 32.$$

## Datums

Vertical coordinate information is referenced to the National Geodetic Vertical Datum of 1929 (NGVD 29).

Horizontal coordinate information is referenced to the World Geodetic System of 1984 (WGS 84).

Elevation, as used in this report, refers to distance above the vertical datum.

## Supplemental Information

Concentrations of chemical constituents in water are given in either milligrams per liter (mg/L) or micrograms per liter (µg/L).

## Abbreviations

1DDV	1-dimensional deep ventilation model
cdf	cumulative distribution function
CTD	conductivity, temperature, depth
CVRMSE	coefficient of variation of the root mean square error
DYRESM	Dynamic Reservoir Simulation Model
GCM	general circulation model
LWC	lower water column
MACA	Multivariate Adaptive Constructed Analog
NRMSE	normalized root mean square error
PNW	Pacific Northwest
RCP	Representative Concentration Pathway
RMSE	root mean square error
SLT	surface layer temperature
SML	surface mixed layer
TKE	turbulent kinetic energy
USGS	U.S. Geological Survey
UWC	upper water column



# Simulation of Deep Ventilation in Crater Lake, Oregon, 1951–2099

By Tamara M. Wood,<sup>1</sup> Susan A. Wherry,<sup>1</sup> Sebastiano Piccolroaz,<sup>2</sup> and Scott F. Girdner<sup>3</sup>

## Abstract

The frequency of deep ventilation events in Crater Lake, a caldera lake in the Oregon Cascade Mountains, was simulated in six future climate scenarios, using a 1-dimensional deep ventilation model (1DDV) that was developed to simulate the ventilation of deep water initiated by reverse stratification and subsequent thermobaric instability. The model was calibrated and validated with lake temperature data collected from 1994 to 2011. Wind and air temperature data from three general circulation models and two representative concentration pathways were used to simulate the change in lake temperature and the frequency of deep ventilation events in possible future climates. The lumped model *air2water* was used to project lake surface temperature, a required boundary condition for the lake model, based on air temperature in the future climates.

The 1DDV model was used to simulate daily water temperature profiles through 2099. All future climate scenarios projected increased water temperature throughout the water column and a substantive reduction in the frequency of deep ventilation events. The least extreme scenario projected the frequency of deep ventilation events to decrease from about 1 in 2 years in current conditions to about 1 in 3 years by 2100. The most extreme scenario considered projected the frequency of deep ventilation events to be about 1 in 7.7 years by 2100. All scenarios predicted that the temperature of the entire water column will be greater than 4 °C for increasing lengths of time in the future and that the conditions required for thermobaric instability induced mixing will become rare or non-existent.

The disruption of deep ventilation by itself does not provide a complete picture of the potential ecological and water quality consequences of warming climate to Crater Lake. Estimating the effect of warming climate on deep water oxygen depletion and water clarity will require careful modeling studies to combine the physical mixing processes affected by the atmosphere with the multitude of factors affecting the growth of algae and corresponding water clarity.

## Introduction

Crater Lake is located in Crater Lake National Park at the crest of the Cascade Range in southern Oregon (fig. 1). The lake partially fills a caldera that formed about 7,700 years ago following the volcanic eruption and collapse of Mt. Mazama. The nearly circular caldera that formed was about 1,220 m deep and 10 km across, and subsequently filled approximately halfway with water. The lake has a maximum depth of 594 m, making it the deepest lake in the United States and eighth deepest in the world. The surface is at 1,883 m elevation and the shoreline is 31 km in length. Crater Lake has no surface outlet and surface inlets are limited to small springs draining the steep caldera walls.

Crater Lake is widely known for its deep blue color and extremely clear water. Summer Secchi depth typically ranges between 25 and 35 m. An ongoing long-term monitoring program was initiated in 1983 in response to concerns that the clarity of the lake might be declining. The lake is extremely biologically unproductive (ultra-oligotrophic), with peak chlorophyll *a* concentrations less than 2 µg/L and low nutrient concentrations (nitrate less than 0.025 mg/L, phosphate less than 0.02 mg/L). The lake is primarily nitrate and iron limited (Groeger, 2007). Most of the available nitrate is located deep in the lake below 200 m, and upward mixing of the deep-water nitrate pool from episodic winter mixing events is estimated to account for more than 85 percent of the seasonal nitrogen input to the upper water column when mixing occurs (Dymond and others, 1996) and influences the autotrophic productivity the following summer. These episodic winter mixing events also bring oxygen-rich surface waters downward and are critical for maintaining oxygen levels at greater than 90 percent of saturation throughout the water column (Crawford and Collier, 2007).

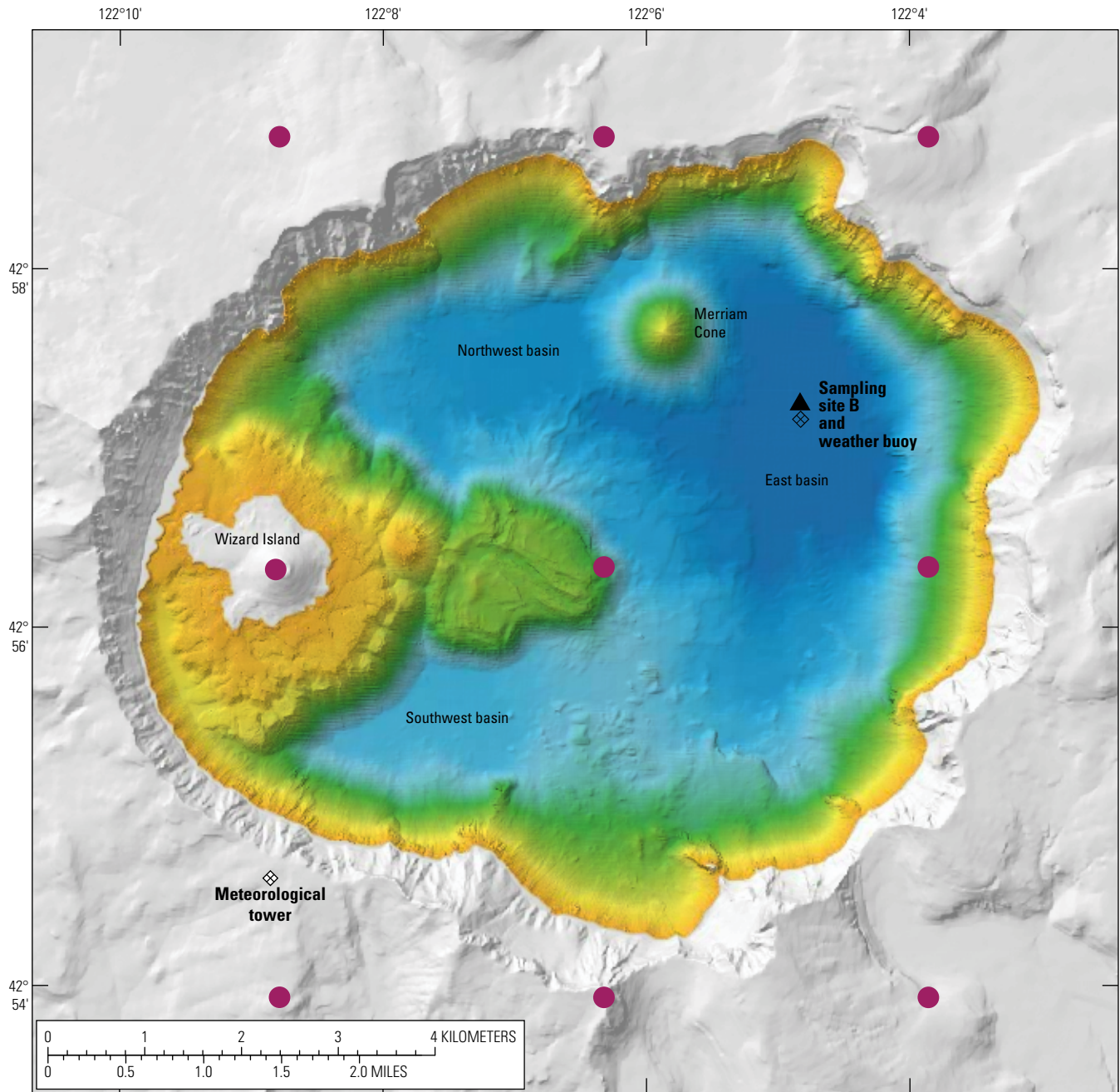
Typical of dimictic lakes, Crater Lake experiences periods of convective vertical mixing in early winter and spring. Between convective mixing periods, strong thermal stratification occurs in summer (warmer water floating on top) and is often reverse stratified in winter (colder water floating on top). Reverse stratification is possible when the upper water column temperatures are less than about 4 °C, the temperature of maximum density at atmospheric pressure.

<sup>1</sup>U.S. Geological Survey.

<sup>2</sup>University of Trento, Italy.

<sup>3</sup>National Park Service, Crater Lake National Park.

## 2 Simulation of Deep Ventilation in Crater Lake, Oregon, 1951–2099

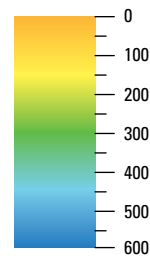


Base modified from U.S. Geological Survey bathymetry and digital elevation model data accessed at <http://oe.oregonexplorer.info/craterlake/bathymetry.html>. Coordinate reference system is NAD 1983 State Plane Oregon South FIPS 3602



### EXPLANATION

Depth below water surface, in meters



● Downscaled MACA climate grid

**Figure 1.** Sampling site and climate model grid, Crater Lake, Oregon.

The lake circulates to a depth of 200–300 m twice each year, in early winter and spring due to wind and convective cooling. However, mixing to the bottom does not occur every winter, but on average every 2–3 years through a process of thermobaric instability when the lake is weakly, reversely stratified (Crawford and Collier, 2007). Because the temperature of maximum density decreases with pressure, it decreases with depth. In a deep lake this fact is of particular importance because it provides the opportunity for strong winds to push colder surface water down to a depth where its temperature is closer to the local temperature of maximum density than the surrounding water. In that situation, the colder surface water is denser than the surrounding water, and continues to sink until it reaches the depth at which it has the same density as the surrounding water, or the bottom of the lake (Boehrer and Schultze, 2008). This type of mixing generally allows surface water to penetrate deeper than convective mixing. Distinct mixing events of this type occurred in Crater Lake in 11 of 22 winters between 1993 and 2014.

The presence of reverse stratification in winter (colder water floating on top of a lake) is essential for thermobarically induced mixing events to occur in Crater Lake (Crawford and Collier, 2007) because it sets up the requisite conditions that allow strong winds to push the upper layer of the lake below the compensation depth (the depth at which the colder surface water has the same density as the surrounding water). However, air and water temperature data from Crater Lake over the last 22 years show that reverse stratification did not occur during the three warmest winters (2001, 2003, and 2005). Because present day meteorological conditions already appear to be near the temperature threshold for reverse stratification, further warming of the climate at Crater Lake could reduce the frequency of winter deep ventilation events or stop them altogether. The absence of deep ventilation and the consequent reduction of the upward nitrate flux into the photic zone could result in a decrease in the already minimal primary production that supports the food web in the lake. A loss of deep ventilation in Crater Lake also would prevent re-oxygenation of the bottom waters. If anoxia in bottom water were to occur, taxa presently living on the lake floor could be lost and nutrients (iron, a co-limiting nutrient; Groeger, 2007) stored in the sediments could be released to the water column. Such changes would result in large-scale ecological impacts on the lake, potentially altering its world-renowned beauty and resulting in a loss of biological communities.

The objective of this study is to assess whether the frequency of climatologically induced deep ventilation events is likely to change in the twenty-first century under warming climate conditions.

## Purpose and Scope

This report presents the results of a partnership between the U.S. Geological Survey (USGS) and the National Park Service to investigate the changes in the frequency of deep

ventilation events in Crater Lake that could be expected in a future, warmer climate. We began by assessing, through calibration and validation, the suitability of a 1-dimensional research-grade vertical lake model recently developed specifically to simulate deep ventilation in Lake Baikal, Russia, for the study of deep ventilation in Crater Lake. We compared the results to simulations produced by a widely used and well-tested 1-dimensional lake model, the DYNAMIC Reservoir Simulation Model (DYRESM), developed by the Centre for Water Research at the University of Western Australia, to demonstrate the importance of using a model specifically designed to incorporate the distinctive and relatively uncommon process responsible for deep ventilation in Crater Lake.

The effects of a future climate were assessed by running the selected model with boundary conditions determined using six climate scenarios from a combination of three GCMs and two RCPs, representing a moderate and extreme scenario of future climate action. The frequency of deep ventilation was assessed over two overlapping 55-year periods during 2007–2099 (2007–2061 and 2045–2099). The change in the frequency of deep ventilation was assessed as a comparison to 55 years of baseline conditions, determined from the same three GCMs.

## Methods

### Datasets

Depth-volume data (hypso-graphic curve) for Crater Lake was derived from a high-resolution (16 million soundings) multi-beam echo sounding survey of the lake completed in 2000 (Bacon and others, 2002).

### Historical Water Quality and Meteorological Data

High frequency meteorological and water quality data have been collected at Crater Lake since 1990. The meteorological datasets used in this study to provide boundary conditions for the lake models included wind speed, air temperature, relative humidity, shortwave solar radiation, and daily accumulation of rain and snow precipitation. Wind speed, air temperature, surface water temperature, and relative humidity were collected year round from a buoy in the lake at site B (fig. 1) at a height of 2-m above water surface at 1-hour intervals. As necessary, small gaps of several days or less were filled with data from a meteorological station located on the crater rim (fig. 1), using regression models developed over periods when both data were available. Solar radiation data were collected at the site on the crater rim. Daily accumulation of rain and snow were collected at Crater Lake National Park Headquarters located below the crater rim, on the south side of Mt. Mazama (fig. 1). The continuous

## 4 Simulation of Deep Ventilation in Crater Lake, Oregon, 1951–2099

water temperature data that were used to calibrate and validate the lake models were collected by thermistors at 10-minute intervals at the discrete target depths of 20, 30, 40, 50, 70, 90, 130, 150, 170, 200, 250, 300, 350, 400, 460, 530 and 580 m at site B between 1992 and 2013.

In addition to the high-frequency thermistor data, water column profiles of temperature and salinity were collected with a conductivity, temperature, and depth sonde (CTD) during discrete sampling events at 1-m depth intervals, primarily between June and October from 1988 to 2013 at site B. The temperature data from these profiles were used to evaluate the turbulent diffusivity profile of the water column, and the salinity data were used to define a salinity-depth relation.

### Climate Data

Downscaled future climate data were used to assess potential climate change effects on the temperature profile and deep-water ventilation of Crater Lake. The University of Idaho provides GCM data from the Coupled Model Intercomparison Project 5 (CMIP5; Taylor and others, 2012) that are statistically downscaled using the Multivariate Adaptive Constructed Analogs (MACA) technique (Abatzoglou and Brown, 2012). Daily air temperature and wind speed data downscaled to a 4-km (1/24 degree in latitude and longitude) spatial resolution were used for the historical period of 1951–2005 and the future period of 2006–2099. At the time that this study began, the number of GCMs for which downscaled data were available was limited. The three GCMs used in this study were selected from those available because they performed well in reproducing the climate of the Pacific Northwest (PNW) region. Specifically, CNRM-CM5 model from the National Centre of Meteorological Research (2014) was the model determined to be the best overall at reproducing various climate metrics in the PNW (Rupp and others, 2013). Two models from the Hadley Centre in the United Kingdom (Met Office, 2014) that differ in the number of vertical atmospheric levels also ranked highly in reproducing PNW climate (Rupp and others, 2013). The HadGEM2-ES model has 38 levels and is closer to the CNRM-CM5 model (31 levels) than the HadGEM2-CC model, which has finer vertical resolution (60 levels). Two available Representative Concentration Pathways, RCP4.5 and RCP8.5, were evaluated for comparison. The RCP4.5 scenario is one of moderate climate mitigation action in which an additional  $4.5 \text{ W m}^{-2}$  of heat is trapped in the earth-atmosphere system, compared to preindustrial conditions, by 2100 (Thomson and others, 2011). The RCP8.5 scenario is more severe, being characterized by a continued heavy reliance on fossil fuels and no implementation of climate policies. In this scenario an additional  $8.5 \text{ W m}^{-2}$  of heat is trapped in the earth-atmosphere system, compared to preindustrial conditions, by 2100 (Riahi and others, 2011). The bounding coordinates designating the area over Crater Lake were  $42.89613^{\circ}\text{N}$  to  $42.97946^{\circ}\text{N}$  and  $122.1472^{\circ}\text{W}$  to  $122.0639^{\circ}\text{W}$ , and this region included nine

MACA grid points (fig. 1). The downscaled air temperature and wind speed from the nine grid points were averaged for each day to acquire daily time-series sets representing conditions at Crater Lake as simulated by the three GCMs.

### Models

The selection of the lake model was critical to the success of this study. Deep ventilation in Crater Lake resulting from thermobaric instabilities is a basin-scale process, which in principle would require a computationally intensive, 3-dimensional model to simulate the fundamental equations of motion. Such a model would require a large amount of data for proper calibration and validation and would be difficult to run through decades of simulations, even with the currently available high performance computational resources. The 1-dimensional deep ventilation model we used (referred to as 1DDV in this report) was developed to efficiently simulate the deep ventilation process triggered by thermobaricity in Lake Baikal by reducing the problem to a 1-dimensional, parameterized vertical energy budget in which the mechanical energy available in the wind is used to move a volume of surface water against a stable density gradient (Piccolroaz, 2013; Piccolroaz and Toffolon, 2013; fig. 2A). The 1DDV model requires a minimum of external forcing input data: water temperature at the surface, wind speed, and wind duration. The 1DDV model does not calculate the surface heat balance; rather, water temperature averaged over the thickness of the model surface layer (herein denoted surface layer temperature, or SLT) must be supplied as a boundary condition for the vertical temperature profile. In addition to measured inputs and calculable model parameters, the 1DDV model requires a reference turbulent diffusivity profile, hydrothermal heat input profile, the hypsometric curve (the relation between depth and water volume), salinity profile, and calibration parameters used to describe energy transfer from the wind to the lake surface layer and the degree of mixing between lake layers. The 1DDV model successfully simulated the deep-water renewal process in Lake Baikal, but it has not been tested in a smaller lake.

Two closure relations are introduced to evaluate the wind energy input at the surface and the volume of water involved in the wind-induced deep downwelling. These relations are at the core of the model and have been derived by schematizing the downwelling process as a layer of water that is accelerated into horizontal motion by the available wind energy input and eventually is forced to move downward along the shoreline boundary (Boehrer and Schultze, 2008). Wüest and others (2005) suggested that deep downwellings in Lake Baikal are likely to be driven by along-shore winds that, given the large dimension of the lake, can cause Ekman transport (National Atmospheric and Space Administration, 2015) of the surface wind-driven layer of water perpendicular to the wind stress and toward the shoreline. Because Crater Lake is smaller than Lake Baikal, a surface Ekman layer is not expected to fully

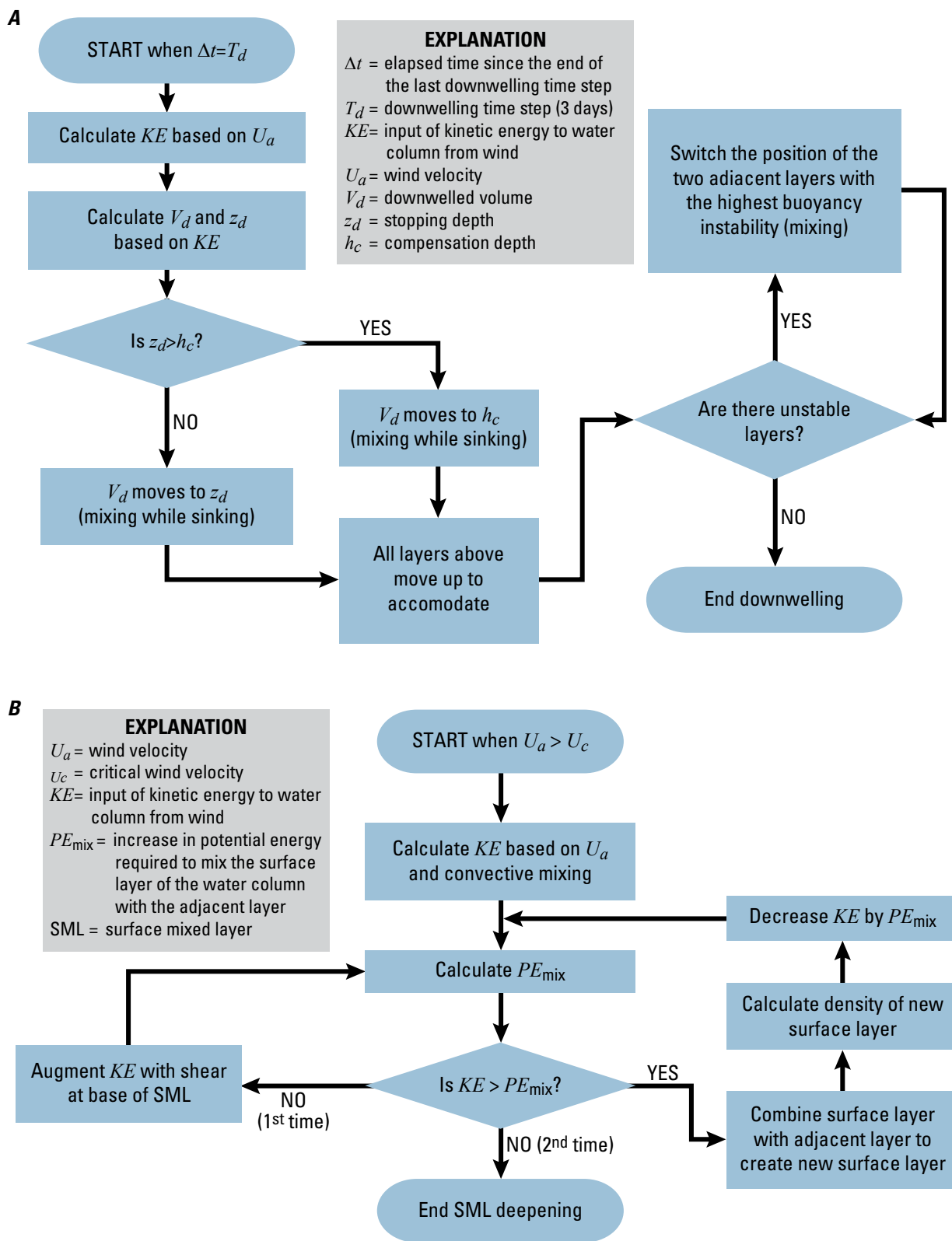


**Figure 2.** Approach used to convert wind stress to water column mixing in the 1-dimensional deep ventilation model (1DDV) and the DYnamic REservoir Simulation Model (DYRESM). (A) Deepwater renewal in 1DDV, and (B) surface mixed layer deepening in DYRESM. The steps have been simplified to emphasize the important differences in approach between the two models.

## 6 Simulation of Deep Ventilation in Crater Lake, Oregon, 1951–2099

develop, and the acceleration of the surface water is likely closer to parallel to the wind stress. As a first approximation, however, the same downwelling closure relations of 1DDV can be used for Crater Lake because the process is set in motion by the wind in both lakes. As in Lake Baikal, buoyancy instabilities due to the thermobaric effect play an important role in determining the deep ventilation process in Crater Lake (Crawford and Collier, 2007), thus making 1DDV particularly well suited to investigate the renewal of deep water in the lake.

As modeled with 1DDV, a lake is divided into a number of layers of equal volume, and a Lagrangian-based algorithm is used to rearrange these volumes to simulate the vertical displacement of water due to deep downwelling and convective mixing. For the simulation of deep downwellings, a finer spatial resolution is used by dividing each volume into a number of subvolumes, with a reasonable increase of the computational cost. The wind energy input to the lake (evaluated over a 3-day period) is compared to the energy that is required to displace the upper volume of water downwards to its compensation depth (the depth where the sinking volume has the same density of the surrounding water). If the energy input is sufficiently large, which is generally the case when the water column is weakly inversely stratified and the wind is sufficiently strong, the downwelling volume is displaced to a point below the compensation depth. There, the sinking volume is heavier than surrounding water, and thus will continue to move downward until it either reaches water of the same temperature or the bottom of the lake. In contrast, shallow convective mixing occurs when the energy input is low or the lake is strongly stratified: the sinking volume is displaced to a depth shallower than the compensation depth, where it is lighter than surrounding water and due to positive buoyant forces is displaced upward again. A limited exchange with surrounding water occurs, but not full mixing, as the volume is moved along the vertical during either deep or shallow downwelling, as well as during vertical rearrangement of subvolumes due to the stabilization of unstable regions of the water column.

To elucidate the atypical nature of the deep ventilation process in Crater Lake further, the well-documented lake model DYRESM (fig. 2B) was used to simulate 6 years of calibration data, and the results were compared to the 1DDV simulation. The DYRESM model is a 1-dimensional hydrodynamic model for lakes and reservoirs developed at the University of Western Australia and used in 59 countries at the time of this writing (Imerito, 2014). The use of the model is limited to situations in which the 1-dimensional assumption is valid; that is, situations in which density stratification is strong enough to provide a strong restoring force to perturbations in the isopycnals resulting from wind energy input at the surface and therefore the isopycnals remain nearly horizontal. DYRESM is Lagrangian-based; the lake

is divided into horizontal layers with uniform properties but varying thicknesses that are determined dynamically to adequately resolve vertical gradients. DYRESM solves the surface heat, mass, and momentum balance; therefore, input data requirements include solar radiation, air vapor pressure and temperature, wind speed, and precipitation. DYRESM simulates the vertical temperature and salinity profile based on surface boundary conditions and hydrothermal inputs, which are modeled as point sources to the deep water column.

The defining structure of the upper water column in DYRESM is the surface mixed layer (SML). Mixing in the upper part of the water column is based on a budget for the turbulent kinetic energy (TKE) of the SML (Tucker and Green, 1977). Wind shear stress is converted to TKE that is used to deepen the mixed layer by entraining adjacent layers if there is enough TKE to overcome the buoyancy forces of a stable water column. Thus, the total TKE input to the water column at every time step (daily for this study) is used to deepen the mixed layer and in the process homogenize the density of the mixed layer. The amount of TKE available is compared to the potential energy (PE) that must be overcome in order to completely mix layers with denser water into the SML. The efficiency with which TKE accomplishes the mixing is controlled through parameters that are set to default values based on well-documented empirical relations. When the assumption of 1-dimensionality is satisfied, the developers state that the model produces an accurate solution without calibration (Imerito, 2014).

It stands to reason that these two models would produce different simulated responses of Crater Lake to the same wind forcing and, further, that each would perform better in some circumstances. DYRESM has been shown to perform well in simulating convective mixing through entrainment of adjacent layers and deepening of the SML, especially during the erosion of summertime thermally stratified conditions, but deep ventilation due to thermobaric instabilities is a fundamentally different process. Therefore, the differences between the results obtained from the models are instructive.

## Data Processing

### Historical Water-Quality and Meteorological Data for the 1-Dimensional Deep Ventilation Model

The measured data inputs to the 1DDV model included daily average SLT data and daily average wind-speed data. Measured vertical temperature profiles were used as initial conditions. Based on these data needs, we identified three periods for simulation with the 1DDV model that were free of large data gaps: (1) from August 13, 1994, to August 14, 1999, (2) from September 23, 2000, to June 27, 2006, and (3) from

August 25, 2008, to June 30, 2011. Daily values of wind speed and SLT were used to be consistent with the temporal resolution of the climate datasets. The computational time step of the model was 12 hours.

Surface water temperature was measured at the buoy (at approximately 2 m depth), but this temperature was not appropriate to be used as the model boundary condition because the surface layer of the model has a thickness of about 10 m. The water temperatures measured under the buoy were also contaminated by heating of the buoy, especially during low-wind events in summer (R.W. Collier, Oregon State University, written commun., 2015). Therefore, the SLT time series used as the upper boundary condition was the temperature measured at 20 m depth (T20), which corresponds to the shallowest thermistor. This measurement is sufficiently far from the surface to exclude the direct contribution of short-term variations of the heat flux components at the lake-atmosphere interface, but close enough to the surface to capture the residual effect of the overall heat exchange and, thus, it proved to be more suitable than the buoy temperature as the thermal condition of the upper layer of the lake. During wintertime reverse-stratified conditions that are most important in this study, the assumption that T20 can represent SLT is appropriate because the surface mixed layer is usually deeper than 20 m; during stratified conditions in summer, this assumption is likely to underestimate SLT, but is still reasonable.

Although the target depth of the shallowest thermistor was 20 m, most of the data were collected at a depth other than 20 m, ranging between 15 and 36 m, depending on the deployment. When the shallowest thermistor data were collected at a depth other than 20 m, the T20 was determined by linear interpolation between the surface buoy and the shallowest thermistor data. When interpolation to 20 m depth was required during strongly stratified summer conditions (during which the epilimnion was warm and thin), and when the uppermost thermistor was installed beneath the thermocline, the interpolated values substantially overestimated the temperature at 20 m. Occasional summertime gaps in the thermistor data, when the thermistors were not in the water, were filled with CTD profile data by linear interpolation, which resulted in a loss of variability in some summer months. The focus of this study, however, was on winter mixing events when variability was unaffected by missing data. The hourly dataset was averaged to a daily dataset for use in the model.

The input wind-speed time series was developed from the meteorological data collected at the buoy in Crater Lake. Wind-speed data were measured at a height of 3 m above water surface, and the values were translated to 10-m values using a logarithmic approximation (Martin and McCutcheon, 1998). The hourly dataset was then averaged to a daily dataset for use in the model.

The initial condition temperature profile at the start of each simulation was extracted from a dataset that combined thermistor data, CTD data, and buoy surface temperature data to provide 1-m temperature profiles interpolated to daily values.

## Historical Water-Quality and Meteorological Data for the Dynamic Reservoir Simulation Model

The measured data inputs to the DYRESM model included daily averaged values of meteorological variables: shortwave solar radiation, cloud cover, air temperature, vapor pressure, wind speed, and daily accumulation of rain and snow precipitation. Based on these data needs, we identified three periods for simulation with the DYRESM model that were free of large data gaps: (1) from January 20, 1993, to August 24, 1999, (2) from September 17, 1999, to August 21, 2007, and (3) from January 18, 2008, to October 28, 2013. Solar radiation data were measured at the meteorological station on the rim. Missing days of data (defined as having less than 20 hourly measurements during the day) were filled with the median value measured on that yearly Julian day over the entire dataset. Cloud cover was not recorded, and was calculated as a function of the ratio of measured daily average solar radiation to the calculated clear sky radiation value (Environmental and Water Resources Institute, 2005) for that Julian day (Crawford and Duchon, 1999; Yang and others, 2010). Air temperature, wind speed, and relative humidity were measured at both the buoy on the lake and at the meteorological station on the crater rim. For these three variables, the data measured at the buoy were used preferentially, and when not available was filled in with data from the rim, corrected using a linear regression between the measurements at both locations. Wind speed data measured at the buoy on the lake at a height of 3 m above the water surface were translated to 10-m values using a logarithmic approximation to the atmospheric boundary layer (Martin and McCutcheon, 1998). Vapor pressure was calculated from relative humidity using the Magnus-Tetens formula (Martin and McCutcheon, 1998). Initial profiles of temperature and salinity were determined from the CTD profile collected most closely in time to the beginning of the simulation.

## Future Climate Data

### Air and Lake Surface Temperature

The future climate datasets of statistically downscaled air temperature and wind speed need to be further downscaled from their regional spatial resolution (1/24 degree in latitude and longitude) to a finer local scale that is representative of the conditions at the lake surface through a bias-correction

## 8 Simulation of Deep Ventilation in Crater Lake, Oregon, 1951–2099

procedure. For air temperature, this bias correction was accomplished with the change factor method, also known as the “delta method” (Diaz-Nieto and Wilby, 2005; Minville and others, 2008), which involves adjusting the GCM time series by assuming that the bias of the GCM compared to measurements on each Julian day in the year as determined during an overlapping historical period applies to the GCM at all other baseline and future times:

$$T_{adj,y} = T_{GCM,y} + (\bar{T}_{obs,h} - \bar{T}_{GCM,h}) \quad (1)$$

where

$\bar{T}_{obs,h}$   
and  $\bar{T}_{GCM,h}$  are the observed and GCM-modeled “mean years” for the same climatological historical period  $h$ , which in this case is the 13-year period 1993–2005 (the mean year is defined by giving to each day of the year the average of all values available in the dataset for that same day); and

$T_{adj,y}$   
and  $T_{GCM,y}$  are the adjusted and GCM-modeled time series of daily air temperature in year  $y$ , where  $y$  can be any year outside the historical period during the GCM baseline (1950–2005) or future climate (2006–2099) period.

Additionally, air temperature needs to be converted into lake temperature at 20 m depth, which is how the SLT, the boundary condition required by the model 1DDV, is defined for this study. The lumped model *air2water* (Piccolroaz and others, 2013) was adopted. The *air2water* model is based on a simplified parameterization of the heat exchanges between a lake and the atmosphere, and is able to simulate daily near-surface lake temperature based only on air temperature as a proxy for the main meteo-climatic variables. The model has been tested on 14 temperate lakes with accuracy comparable to more complex process-based models that require substantially more input data (Toffolon and others, 2014). The *air2water* model also has been used successfully to investigate the feedback between stratification and thermal response of lakes (Piccolroaz and others, 2015). For Crater Lake specifically, the full (eight-parameter) version of the model was used, and the parameters were calibrated using the measured daily average of air temperature and lake temperature at 20 m depth during the historical period 1993–2011. The temperature at 20 m depth sometimes had to be determined with an interpolation between the buoy (2 m) temperature and the uppermost thermistor (at approximately 20 m) (see section, “[Historical Water-Quality and Meteorological Data for the 1-Dimensional Deep Ventilation Model](#)”). When this resulted in unrealistically high values in summer, those values were removed before

calibrating *air2water*. The calibration of *air2water* with this time series of water temperature was successful, resulting in a root mean square error (RMSE) of 0.68 °C between the simulated and measured daily values of T20 over the entire calibration period of 1993–2011. Further, *air2water* was able to capture the inter-annual variability and the long-term trend in T20, particularly in the December–May average (the months that correspond to the time of year when the lake is inversely stratified or only weakly directly stratified [fig. 3]).

The calibrated *air2water* model was used to project T20 using the downscaled air temperature calculated with equation (1), for both the entire baseline period of 1951–2005 and the future conditions period of 2006–2099. Results of the application of *air2water* to the baseline and future scenarios are presented for each of the GCMs in figure 4A–C in terms of the December–May mean, with downscaled baseline and future conditions air temperature. Summary statistics are provided in table 1. The long-term trends in air and water temperature are indicated by the slope of the linear regressions, and show that, as expected, the water temperature does not warm as fast as the air temperature and the interannual variability in the water temperature is less than the interannual variability in the air temperature. Figure 4 indicates how the projected warming of air temperature could affect T20 during the 21st century. Depending on the GCM, the warming trend in water temperature is between 0.013 and 0.019 °C per year in the RCP4.5 scenario and 0.034 and 0.035 °C per year in the RCP8.5 scenario, compared with air temperature warming trends between 0.021 and 0.031 °C per year and 0.055 and 0.060 °C per year, respectively, in the same scenarios.

The long-term trends in T20 for the cold season from December to May directly quantify the effect that a future increase in air temperature is expected to have on the thermal regime of the lake. This effect is evident in the comparison of the mean annual T20 and, more importantly, the mean annual percentage of days with T20 colder than 4 °C for the three GCMs and two RCPs, between the baseline period and future conditions. The CNRM-CM5 GCM projects the lowest average air temperatures for both baseline and future conditions, increasing 2.55 °C, from 4.80 °C (baseline) to 7.35 °C in the RCP4.5 scenario and increasing 4.28 °C, from 4.80 to 9.08 °C in the RCP8.5 scenario (table 1).

By the second half of the 21st century, the annual percentage of days during which the lake is inversely stratified (a necessary condition for thermobaric instabilities to occur) is expected to decrease from 38.9 percent (baseline) to 8.8 percent and 3.4 percent in the RCP4.5 and RCP 8.5 scenarios, respectively. The HadGEM2-CC and HadGEM2-ES GCMs project similar results. HadGEM2-CC projects the highest average air temperatures for both baseline and future conditions, increasing 2.97 °C, from 5.40 °C (baseline) to 8.37 °C in the RCP4.5 scenario and increasing 4.85 °C from 5.40 to 10.25 °C in the RCP8.5 scenario (table 1). Conversely, HadGEM2-ES projects the largest shortening of

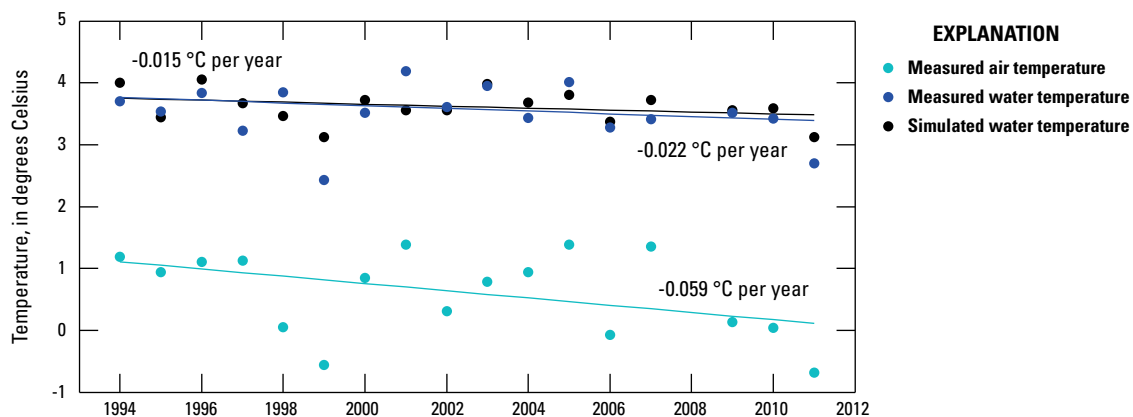


**Figure 3.** December-to-May averages (plotted at January 1) of air temperature and water temperature at 20 meter depth, and water temperature at 20 meter depth simulated by the lumped model *air2water*, during the calibration period 1993–2011 at Crater Lake, Oregon. Multi-annual trends (evaluated using robust linear regression) of air and water temperature also are shown.

**Table 1.** Statistical characteristics of air temperature and water temperature for the historical period of record and for the baseline and future conditions periods from three general circulation models (GCMs) and two representative concentration pathways.

[Water temperature is at 20 meter depth as simulated with the *air2water* model. Abbreviation: °C, degree Celsius]

GCM or measured	Period	Average daily air temperature, $T_{air}$ (°C)	Standard deviation daily air temperature (°C)	Average daily water temperature $T_{20}$ (°C)	Standard deviation daily water temperature (°C)	Annual percentage of days with water temperature less than 4 °C	$T_{20} - T_{air}$ (°C)
Historical period of observations: 1995–1999, 2001–2006, 2009–2011							
Measured	All months	5.03	6.85	5.60	2.48	40.2	0.57
	December to May	0.54	3.89	3.56	0.71	79.0	3.02
Baseline conditions: 1951–2005							
CNRM-CM5	All months	4.80	6.91	5.26	2.37	38.9	0.46
	December to May	0.18	3.99	3.38	1.07	72.8	3.20
HadGEM2-CC	All months	5.40	7.10	5.67	2.43	34.1	0.27
	December to May	0.80	4.30	3.63	0.96	68.0	2.83
HadGEM2-ES	All months	5.10	6.90	5.46	2.36	37.1	0.36
	December to May	0.75	4.23	3.48	0.89	73.3	2.73
Last 55 years of future conditions: 2045–2099, representative concentration pathway 4.5							
CNRM-CM5	All months	7.35	7.04	6.94	2.55	8.8	-0.41
	December to May	2.79	3.93	4.86	0.96	17.5	2.07
HadGEM2-CC	All months	8.37	7.72	7.61	2.90	3.6	-0.76
	December to May	3.23	4.57	5.15	0.96	7.1	1.92
HadGEM2-ES	All months	8.46	7.57	7.67	2.86	2.5	-0.79
	December to May	3.34	4.41	5.26	0.92	5.1	1.92
Last 55 years of future conditions: 2045–2099, representative concentration pathway 8.5							
CNRM-CM5	All months	9.08	7.38	8.07	2.90	3.4	-1.01
	December to May	4.38	4.39	5.83	1.28	6.9	1.45
HadGEM2-CC	All months	10.25	8.15	8.84	3.30	1.3	-1.41
	December to May	4.69	4.69	6.12	1.20	2.7	1.43
HadGEM2-ES	All months	10.14	7.91	8.77	3.19	0.1	-1.37
	December to May	4.90	4.43	6.13	1.00	0.2	1.23

10 Simulation of Deep Ventilation in Crater Lake, Oregon, 1951–2099

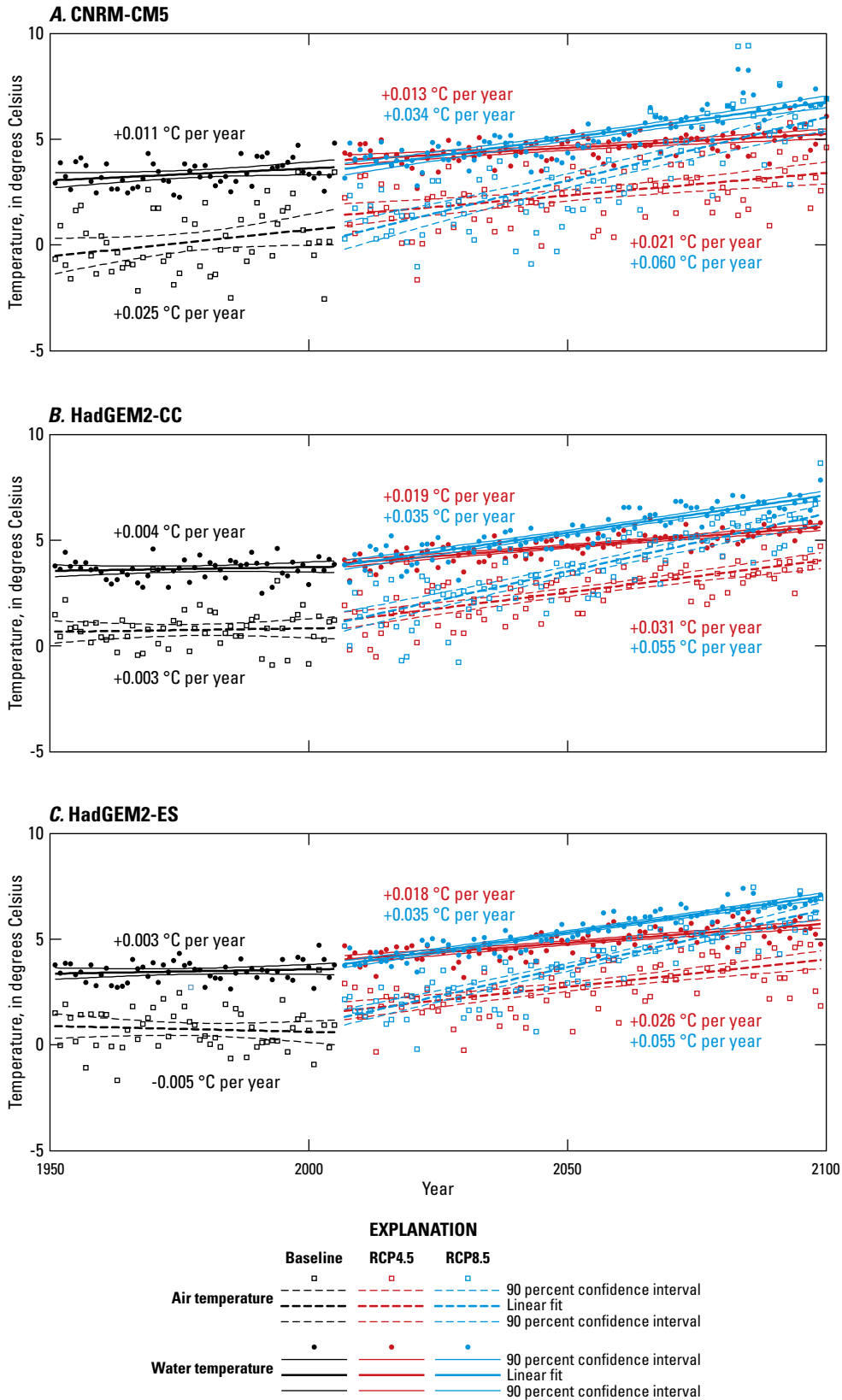


**Figure 4.** December-to-May averages of downscaled air temperature from general circulation models (GCMs), and water temperature at 20 meter depth as determined with the *air2water* model, through baseline (1951–2005) and future climate (2006–2099) conditions at Crater Lake, Oregon. Long-term trends (evaluated using robust linear regression) of air and water temperature also are shown.

the duration of inverse stratification during the second half of the 21st century, with a decrease from the 37.1 percent of the year (baseline) to the 2.5 percent and 0.1 percent in the RCP4.5 and RCP 8.5 scenarios, respectively. The notable decrease in the number of days in the year when T20 is less than 4 °C projected by all GCMs is expected to have strong implications for the general thermo-hydrodynamics of the lake.

The variability in daily air temperature increases with the average temperature, but the projected increase is different among the GCMs. CNRM-CM5 projects the smallest increase in the standard deviation of daily values at 0.13 °C between baseline and RCP4.5 conditions and 0.47 °C between baseline and RCP8.5 conditions. HadGEM2-CC projects the biggest increase in the standard deviation of daily values at 0.62 °C between baseline and RCP4.5 conditions and 1.05 °C between baseline and RCP8.5 conditions. The differences among the average water temperature and the standard deviation of daily water temperature as projected by the GCMs mirror the projected differences in air temperature, but are smaller in magnitude. Given the large differences between the long-term trends in air temperature as determined by the three GCMs and the two RCPs and how closely projected water temperature tracks projected air temperature, the uncertainties in the climate scenarios are likely to dwarf any errors in the application of *air2water* to determine T20.

## Wind Speed

There is no expectation that individual events in the time series of wind speed obtained from a GCM should match those in the measurements during the historical period, but the statistics describing the distribution of wind speed should be as close as possible for the wind speed from the GCMs to represent current conditions. When the cumulative distribution function (cdf) of the wind speed measurements (daily means, 1991–2005) was compared to the cdf of the daily values from the GCMs for the same historical period, there was substantial bias, especially at higher wind speeds, indicating the need for an additional downscaling step aimed at matching local scale measurements (fig. 5). The approach used to downscale wind speed to the lake surface was similar to the statistical downscaling procedure adopted by Piccolroaz (2013). In this case, the future period was divided into 10-year sub-periods ( $p$ ) for which the corresponding cumulative distribution functions of GCM-modeled daily wind speed were evaluated ( $cdf_{GCM,p}$ ). Each cdf was compared to the cdf of the GCM-modeled wind speed during the reference historical period ( $cdf_{GCM,h}$ ), in order to define a change function for

the sub-period ( $r_p$ ) that is defined as the ratio between the two cdfs. This change function was used to modify the cdf of measurements (daily means, to be consistent with the daily data from the GCMs) during the reference historical period ( $cdf_{obs,h}$ ), to create an adjusted cdf ( $cdf_{adj,p}$ ) that would describe the GCM-simulated wind speed for each future sub-period ( $p$ ). To summarize, this technique applies the translation between the cdf of the measurements and the GCM-simulated data during the historical reference period to sub-periods outside the historical reference period in order to obtain downscaled values from the GCM-simulated data. The reference historical period ( $h$ ) was defined as the period when wind speed measurements and baseline data from the GCMs overlapped (1991–2005). The whole procedure can be summarized as follows:

$$cdf_{adj,p} = cdf_{obs,h} r_p = cdf_{obs,h} \frac{cdf_{GCM,p}}{cdf_{GCM,h}} \quad (2)$$

The final adjusted wind speed ( $W_{adj,p}$ ) was computed from the adjusted cdf for the sub-period by applying the quantile-mapping approach (Panofsky and Brier, 1968):

$$W_{adj,p} = cdf_{adj,p}^{-1} \left( cdf_{GCM,p} \left( W_{GCM,p} \right) \right) \quad (3)$$

where

$$\begin{aligned} W_{GCM,p} & \text{ is the daily series of GCM-modeled wind} \\ & \text{ speed for the sub-period } p, \text{ and} \\ cdf_{adj,p}^{-1} & \text{ is the inverse of } cdf_{adj,p}. \end{aligned}$$

Results of the downscaling are presented in figure 5 in terms of maximum, mean, and minimum annual wind speed for both historical and future periods. The projected changes in average daily wind speed and average annual maximum wind speed between baseline and future conditions are small (table 2). The CNRM-CM5 GCM projects the 50th percentile wind speed to increase slightly between baseline conditions and either RCP, from 3.71 to 3.77 m/s, whereas the HadGEM2-CC GCM projects 50th percentile wind speed to decrease slightly, from 3.73 to 3.59 m/s in the RCP4.5 scenario, and from 3.73 to 3.52 m/s in the RCP 8.5 scenario. HadGEM2-ES projects decreasing average wind speeds of similar magnitude. These results suggest that changes in the frequency of deep ventilation in Crater Lake as simulated by these future climate scenarios are likely to be mainly attributable to the projected changes in air temperature rather than wind speed.

12 Simulation of Deep Ventilation in Crater Lake, Oregon, 1951–2099

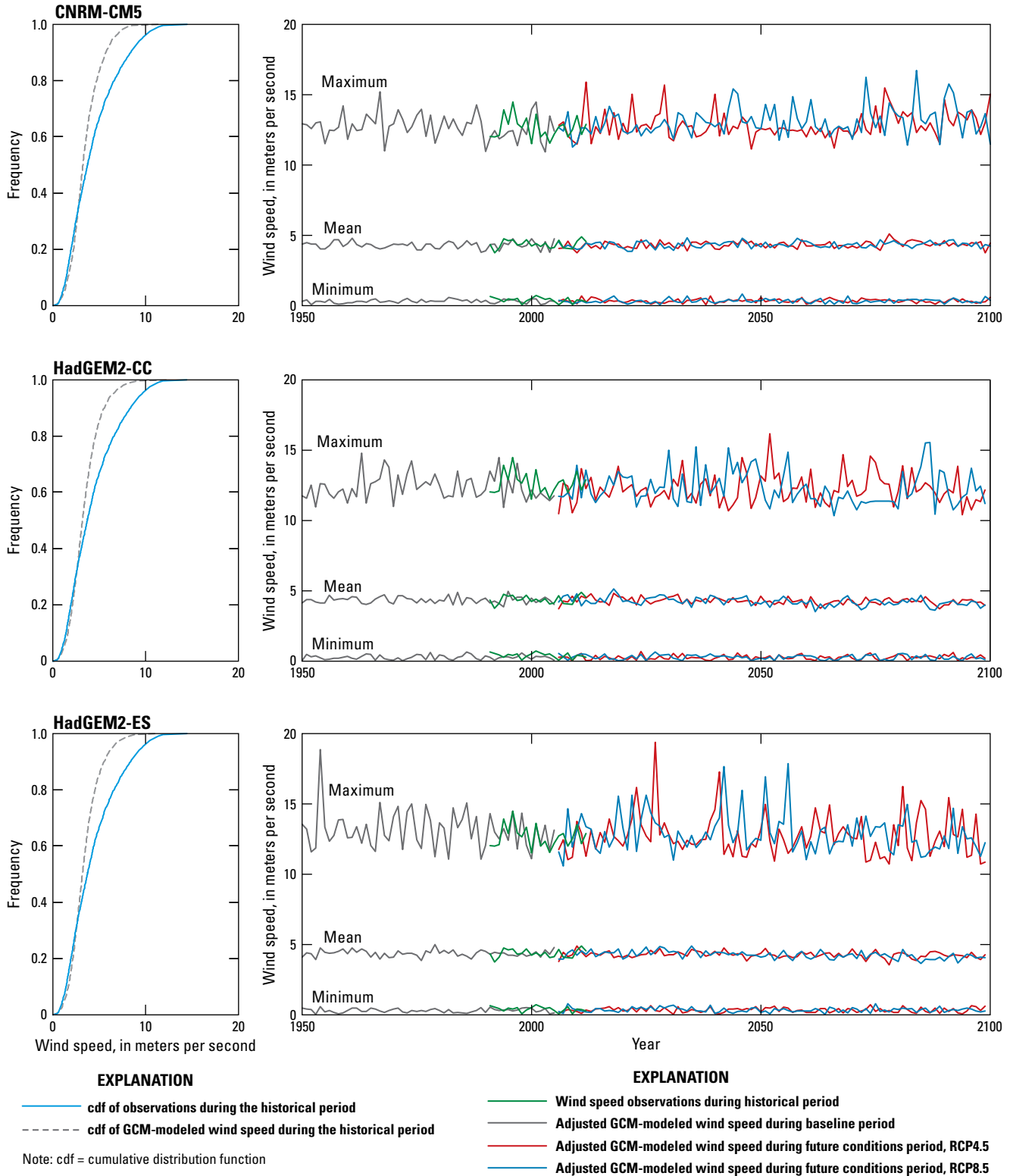


**Figure 5.** Cumulative distribution functions of measured and simulated daily wind speed for the common historical period 1991–2005, and the original and adjusted minimum, mean, and maximum wind speed from three general circulation models and two representative concentration pathways during baseline (1951–2005) and future (2006–2099) conditions at Crater Lake, Oregon.

**Table 2.** Statistical characteristics of wind speed for the historical period of record and for the baseline and future conditions periods from three general circulation models (GCMs) and two representative concentration pathways.

GCM or measured	Period	Daily wind speed, in meters per second			
		50th percentile	75th percentile	90th percentile	Maximum
Historical period of observations: 1995–1999, 2001–2006, 2009–2011					
Measured	All months	3.81	6.10	8.57	14.47
	December to May	4.67	7.24	9.25	13.04
Baseline conditions: 1951–2005					
CNRM-CM5	All months	3.71	5.84	8.28	15.19
	December to May	4.38	6.96	9.14	14.47
HadGEM2-CC	All months	3.73	5.89	8.43	14.79
	December to May	4.36	7.09	9.26	14.79
HadGEM2-ES	All months	3.73	5.98	8.48	18.86
	December to May	4.39	7.14	9.32	18.86
Last 55 years of future conditions: 2045–2099, representative concentration pathway 4.5					
CNRM-CM5	All months	3.77	5.93	8.33	15.45
	December to May	4.52	6.99	9.12	14.57
HadGEM2-CC	All months	3.59	5.69	8.27	16.16
	December to May	4.26	6.96	9.08	14.58
HadGEM2-ES	All months	3.60	5.77	8.19	16.24
	December to May	4.41	7.01	8.97	16.24
Last 55 years of future conditions: 2045–2099, representative concentration pathway 8.5					
CNRM-CM5	All months	3.77	5.94	8.30	16.70
	December to May	4.57	7.01	9.10	15.11
HadGEM2-CC	All months	3.52	5.57	8.14	15.53
	December to May	4.25	6.87	9.05	15.50
HadGEM2-ES	All months	3.54	5.65	8.01	17.84
	December to May	4.26	6.79	8.79	16.29

## One-Dimensional Lake Temperature Modeling

### One-Dimensional Deep Ventilation Model

Density in Crater Lake is a function of temperature, pressure, and salinity. Ideally, the salinity concentration profile that results from the balance of hydrothermal inputs at the bottom and freshwater inputs at the surface would be part of the model solution. For the purpose of calculating density in the 1DDV model, however, the change in the salinity profile through time is small. Instead, an average salinity profile was calculated from CTD profiles collected at site B (fig. 1) and

assumed invariant. A fourth order polynomial fit to the average salinity profile was used in the model and was assumed time-invariant (fig. 6). This profile increases nearly linearly with depth below 200 m, from about 104.5 to about 108 mg/L at the bottom, a gradient of  $8.75 \times 10^{-3}$  (mg/L)/m, comparable to Crawford and Collier (2007). Above 200 m depth, salinity increases more steeply with depth, from about 104 mg/L at the surface (fig. 6).

### Initial Values of Calibration Parameters

The closure relations at the core of the model require the calibration of two parameters,  $\xi$  and  $\eta$ , which are mainly dependent on the morphological properties of the lake. Scaling

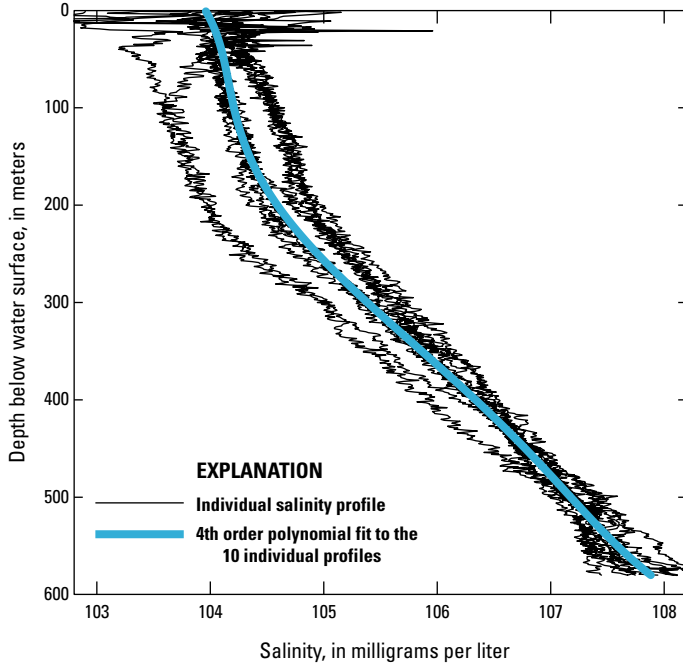


**Figure 6.** Ten salinity profiles at Site B, Crater Lake, Oregon, collected between July and September, 1991–1998, and a 4th order polynomial fit to the average of the profiles.

arguments were used to determine starting values for these parameters. The first parameter,  $\xi$  [(kg/m<sup>2</sup>)/s], is used to evaluate the external specific energy input from wind to the lake surface layer (Piccolroaz and Toffolon, 2013):

$$e_w = \xi \sqrt{C_D} W \sim \frac{\tau_w A_w}{HB} \quad (4)$$

where

- $C_D$  is the wind drag coefficient,
- $W$  is the wind speed at 10-meters above the lake surface,
- $H$  is the depth of the wind-affected layer approximated as the Ekman layer depth,  $\frac{0.4u_*}{f}$ ,
- $B$  is the horizontal scale of the wind-affected area (assumed to be the lake diameter, 8,200 m),
- $A_w$  is the water surface area affected by wind (taken to be the lake surface area,  $53 \times 10^6$  m<sup>2</sup>),
- $\tau_w$  is the wind shear stress,  $\tau_w = \rho_a C_D W^2$
- $\rho_a$  is air density,
- $\rho_0$  is water density,
- $f$  is the Coriolis frequency ( $9.94 \times 10^{-5}$  per s at Crater Lake's latitude of  $42.95^\circ$ N), and
- $u_*$  is the friction velocity,  $u_* = \sqrt{\frac{\tau_w}{\rho_0}}$ .

Substituting for  $H$  and  $\tau_w$  equation (4) can be rewritten:

$$\xi \sim \frac{\sqrt{\rho_a \rho_0} A_w f}{0.4B} \quad (5)$$

The starting value of  $\xi$  was calculated as 56 (kg/m<sup>2</sup>)/s.

The second parameter,  $\eta$  [km h], is used to estimate the sinking volume during a downwelling event (Piccolroaz and Toffolon, 2013):

$$V_d = \eta C_D W^2 \Delta t_w \sim HBU \Delta t_w \quad (6)$$

where

- $\Delta t_w$  is the wind duration, and
- $U$  is the mean water velocity within the wind-driven layer (assumed proportional to  $u_*$ ).

Equation 6 yields the following expression for  $\eta$ :

$$\eta \sim \frac{0.4\rho_a B}{\rho_0 f} \quad (7)$$

Assuming the full surface area of Crater Lake was wind-affected, the starting value of  $\eta$  was calculated as 0.01128 km h.

Two other calibration parameters in 1DDV determine the degree of mixing that occurs between layers. When adjacent layers are exchanged in the process of simulating convective mixing, the parameter  $c_{mix}$  allows for a partial exchange of water between the adjacent layers (and proportional modification of tracer concentrations). When deep downwelling and ventilation occurs and a surface volume moves downward, the parameter  $c'_{mix}$  accounts for a partial exchange between the sinking volume and the surrounding layers. Generally,  $c_{mix}$  is expected to be greater than  $c'_{mix}$ , reflecting the fact that deep downwelling is a relatively rapid process.

## Reference Diffusivity Profile

The reference turbulent diffusivity profile required by the model was determined using a modification of the heat budget method (Sweers, 1970; Powell and Jassby, 1974; Jassby and Powell, 1975) that accommodated hydrothermal inputs, expressed as:

$$K_{z,r} = - \left( A_z \frac{\partial T_z}{\partial z} \right)^{-1} \left( \frac{dH_z}{dt} - G_z \right) \quad (8)$$

where

- $K_{z,r}$ ,  $A_z$ , and  $T_z$  are the reference turbulent diffusivity, cross-sectional area, and temperature, respectively, at depth  $z$ ;

$H_z$  is the heat content at depth  $z$  defined as:

$$H_z = \int_{z_m}^z T(z', t) A(z') dz' \quad \text{and} \quad (9)$$

$G_z$  is the total hydrothermal heat input between the maximum depth  $z_m$  and depth  $z$ :

$$G_z = RB(z) (\rho_0 c_p)^{-1} \quad (10)$$

$B(z)$  is the “effective” bottom area between the maximum depth  $z_m$  and depth  $z$ ; that is, the area through which the flux of hydrothermal heat  $R$  in  $\text{W}/\text{m}^2$  occurs; and  $\rho_0$  and  $c_p$  are the density and specific heat of water, respectively.

Implicit in equation 10 is the assumption that the hydrothermal flux  $R$  is constant; that is, hydrothermal inputs as a function of depth are proportional to the circumscribed bottom area at each depth. This influences the shape of the turbulent diffusivity profile, but there is no basis for a different assumption. Because radiative heating is not included, equation 8 is only valid below the depth of maximum penetration of the radiative flux of heat from the surface. Additionally, the CTD temperature profiles that were used to calculate the terms in the equation did not normally go to the maximum depth in the lake; therefore, the valid range of integration was limited to depths below 50 m to avoid radiative fluxes and above 550 m, a depth attained by most temperature profiles.

The temperature profile in Crater Lake has a temperature minimum ( $T_{min}$ ) at a depth ( $z_{min}$ ) below the seasonal thermocline, located generally between 250 and 350 m depth. The small increase in temperature with depth below  $z_{min}$  is a consequence of hydrothermal inputs (McManus and others, 1992). The calculation of terms in equation 8 was limited to profiles between July and September of each year, when the change in heat content below  $z_{min}$  could be attributed to hydrothermal inputs alone, under the assumptions that the diffusive fluxes across  $z_{min}$  are zero and exchange with water from the upper water column does not occur during these months. Under these assumptions, the change in heat content in the deep water column between an initial July profile and a final September profile was estimated as:

$$\Delta H_{deep} = \rho_0 c_p (H_{\bar{z}, final} - H_{\bar{z}, initial}) \quad (11)$$

where

$\bar{z}$  was the midpoint between depth of minimum temperature in the initial and final profiles.

The change in heat content calculated in this way had an average value of  $1.4 \text{ W}/\text{m}^2$  over 19 years, when normalized to the bottom area below 350 m depth, as compared to the previous estimate of  $1 \text{ W}/\text{m}^2$  (McManus and others, 1993). The hydrothermal flux calculated in this way varied substantially from year to year (table 3). Whether this indicates a true variation in hydrothermal inputs or 3-dimensional effects related to the transport of hydrothermal fluids between the primary source in the south basin and the location of site B (fig. 1) is unknown, but for the purpose of calculating diffusivity, a different value of the hydrothermal heat flux  $R$  in equation 10 was assigned to each year by dividing the calculated change in heat content in that year by the bottom surface area between 400 and 550 m depth. An upper limit of 400 m was used instead of 350 m as in McManus and others (1993) because it was below the deepest value of  $z_{min}$  in the profiles.

In the metalimnion above  $z_{min}$  the change in heat content through summer is expected to be positive as a result of diffusive transport of heat from the surface downward. However, the change in heat content between 150 m (below the thermocline) and  $\bar{z}$ , calculated in a manner analogous

**Table 3.** Rate of change in heat content in the deep and mid water column, and the calculated hydrothermal flux between July and September, Crater Lake, Oregon, 1990–2013.

[Hydrothermal flux  $R$  is calculated based on bottom surface area below 350 meters depth. **Abbreviations:** J/d, joule per day;  $\text{W}/\text{m}^2$ , watt per square meter]

Year	Deep ( $\times 10^{12}$ J/d)	$R$ ( $\text{W}/\text{m}^2$ )
1990	1.43	0.56
1991	1.00	0.39
1994	3.18	1.25
1995	4.98	1.96
1996	1.07	0.42
1998	6.55	2.58
1999	3.85	1.51
2000	1.96	0.77
2003	8.57	3.37
2004	5.48	2.15
2005	2.42	0.95
2006	-0.24	-0.09
2007	2.32	0.91
2008	3.80	1.49
2009	7.25	2.85
2010	4.06	1.59
2011	3.44	1.35
2012	2.42	0.95
2013	3.03	1.19
Mean	3.50	1.38

to equation 11, resulted in changes that were positive and negative, implicating horizontal transport and lateral heterogeneity. Ravens and others (2000) encountered similar difficulties in calculating  $K_{z,r}$  using the heat budget method in Lake Baikal. A mean  $K_{z,r}$  profile was obtained by averaging only those years in which the overall change in heat content between 150 m depth and  $\bar{z}$  was positive, indicating diffusive transport, and removing the remaining few spurious negative values from the profiles before averaging. The final profile above 350 m depth was based on July and September profiles in 9 years; the profile below 350 m was based on July and September profiles in 19 years (fig. 7). The resulting profile shows an increase in diffusivity in the deep lake below the temperature minimum, where hydrothermal inputs make the water column marginally stable (McManus and others, 1993). The profile is broadly consistent with the previous estimates of a turbulent diffusion coefficient between  $10^{-4}$  and  $10^{-3}$  m<sup>2</sup>/s (McManus and others, 1993), although, because it is calculated over summer, the profile could be an underestimate of diffusive mixing during the winter. McManus and others (1993) calculated values for the summer between  $6 \times 10^{-4}$  and  $8 \times 10^{-4}$  m<sup>2</sup>/s at depths from 250 to 420 m, about a factor of 2 smaller than the estimate of  $2 \times 10^{-3}$  calculated for February.

Because the diffusivity profile typically is characterized by a marked seasonality and may undergo significant inter-annual variability due to changes in external forcing,

the model is provided with a simple module to dynamically reconstruct the temporal evolution of  $K_z$ . At every computational time step,  $K_z$  is derived building on well-known empirical relationships of the type (for example, Munk and Anderson, 1948; Pacanowski and Philander, 1981):

$$K_z = \frac{K_{z,r}}{(1 + aRi)^c} K_{z,bg} \quad (12)$$

where

- $K_{z,r}$  is the reference diffusivity profile;
- $K_{z,bg}$  is a background value (set equal to  $1 \times 10^{-5}$  m<sup>2</sup>/s, consistent with typical values suggested by Pacanowski and Philander [1981]); and
- $Ri$  is the Richardson number and  $a$ ,  $b$ , and  $c$  are positive parameters.

For the purpose of calculating the Richardson number, the square of the vertical velocity gradient is calculated as the sum of a background value, an internal wave contribution proportional to the Brunt-Vaisala frequency, and a wind shear contribution based on the law of the wall (Mellor, 1989; see also Piccolroaz and Toffolon, 2013, appendix A for details). Within the uppermost layer of the lake (that is, within the Ekman layer)  $K_z$  is imposed to be uniform and equal to

$$K_{z,surf} = \frac{1}{f} \left( \frac{\rho_a C_D}{\rho_0 k} \right)^2 W^2 \quad (13)$$

where

- $k$  is a constant that is in the range  $1 \times 10^{-2} \leq k \leq 4 \times 10^{-2}$  (Kullenberg, 1976).

### Calibration

Historical data between September 23, 2000 and August 3, 2006, the “middle” period of available data, were used for model calibration. Crater Lake was organized into 37 layers of equal volume of 0.5 km<sup>3</sup>, and sub-volumes were set equal to 0.1 km<sup>3</sup>. The 37 layers were centered at depths between 5 and 554 m. Calibration began by using the calculated starting values of 56 (kg/m<sup>2</sup>)/s and 0.01128 km h for  $\xi$  and  $\eta$ , respectively, and the mixing percentages of 0.6 percent between ambient and downwelling volumes and 10 percent between unstable sub-volumes that were used for Lake Baikal (Piccolroaz and Toffolon, 2013). Equation 13 was evaluated for four values of  $k$  within the acceptable range: 0.01, 0.02, 0.03, and 0.04; a value of 0.02 was selected for further model calibration.

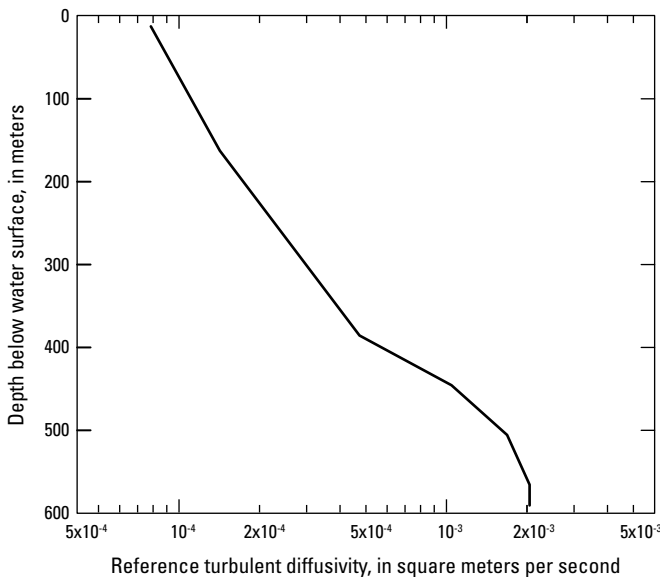


**Figure 7.** Reference turbulent diffusivity profile for the 1-dimensional deep ventilation model of Crater Lake, Oregon.

Several combinations of  $\xi$ ,  $\eta$ ,  $c'_{mix}$  and  $c_{mix}$  values were considered. The calibration process started by considering  $\xi$  values ranging from 1 to 56 (kg/m<sup>2</sup>)/s to determine a minimum value required to translate the measured wind into enough kinetic energy to induce mixing; this minimum value was approximately 7 (kg/m<sup>2</sup>)/s. Next, several combinations of  $\xi$  and  $\eta$  were considered by incremental adjustments of  $\xi$  by approximately 5 (kg/m<sup>2</sup>)/s and  $\eta$  by approximately 0.00077 km h. When a good set of parameter values that captured the general timing and magnitude of deep ventilation events was attained ( $\xi$  of 20–30 (kg/m<sup>2</sup>)/s and  $\eta$  of 0.003–0.008 km h), the parameter increments were further refined and adjustments to the mixing parameters were made based on inspection of simulated temperature time series at 16 depths in the lake where temperature was measured. The final combination of parameter values that provided the best overall simulation of temperature at depths between 20 and 530 m and which best captured the occurrence and magnitude of deep ventilation events, determined by minimizing the RMSE of December–June changes in lower lake heat content, was:  $\eta$  equal to 0.00386 km h,  $\xi$  equal to 28 (kg/m<sup>2</sup>)/s,  $c_{mix}$  equal to 10.0 percent, and  $c'_{mix}$  equal to 9.0 percent (table 4).

The resulting calibrated model had a tendency to simulate a deeper-than-observed thermocline (that is, warmer temperatures than measured above 70 m depth) in late summer and colder temperatures than measured in the metalimnion down to 200 or 250 m depth in late spring and summer, but captured the overall shape of the thermal profile and its seasonal changes well (figs. 8, 9, and 10). The winter months of reverse stratification generally are characterized by a thicker mixed layer in the thermistor data than is simulated by the model. Performance statistics for the calibrated model

**Table 4.** Calibration parameters for the 1-dimensional deep ventilation model of Crater Lake, Oregon.

[Abbreviations: km, kilometer; h, hour; kg, kilogram; m, meter; s, second; –, no units]

Parameter	Value	Units
$\eta$	0.00386	km h
$\xi$	28	(kg/m <sup>2</sup> )/s
$c_{mix}$	10.00	percent
$c'_{mix}$	9.00	percent
$k$	0.02	–

simulations of temperature compared to thermistor data at target depths are presented in table 5. Maximum values of bias (positive), RMSE, and the coefficient of variation of the RMSE (CVRMSE) between the simulated and measured temperature were between 40 and 70 m depth, a result of the simulated depth of the thermocline being too great in summer, and the simulated base of the mixed layer being too shallow in winter (figs. 8 and 9).

At the base of and below the seasonal thermocline the model simulated the rapid changes in temperature associated with a deepening mixed layer in the cooling phase of the seasonal cycle, but the extremes in temperature were smaller than measured (between 150 and 250 m in fig. 11). In the deep lake, below 350 m, the abrupt drop in temperature of a fraction of a degree associated with deep ventilation events in 2004 and 2006 were well simulated. At 530 m, the deep ventilation event that is mild in the 2002 measurements was simulated as a somewhat stronger event by the 1DDV model, penetrating to the deepest simulation layer representing the bottom of the lake.

**Table 5.** Goodness-of-fit statistics at thermistor target depths for temperature simulated with the 1-dimensional deep ventilation model, Crater Lake, Oregon, 2000–2006.

[RMSE: Root-mean-square error. NRMSE: Normalized root-mean-square error (RMSE divided by the range of the observations). CVRMSE: Coefficient of variation of the root-mean-square error (RMSE divided by the mean of the observations). Abbreviation: °C, degrees Celsius]

Depth	Bias (°C)	RMSE (°C)	NRMSE	CVRMSE
20	-0.12	0.31	0.03	0.06
40	0.26	0.66	0.11	0.14
50	0.27	0.68	0.13	0.15
70	0.15	0.44	0.12	0.11
90	0.06	0.30	0.10	0.08
110	0.01	0.24	0.11	0.06
130	0.00	0.20	0.10	0.05
150	0.02	0.17	0.11	0.05
170	0.03	0.16	0.12	0.04
200	0.04	0.13	0.12	0.04
250	0.05	0.09	0.13	0.03
300	0.07	0.08	0.16	0.02
350	0.07	0.08	0.24	0.02
400	0.06	0.07	0.27	0.02
460	0.04	0.06	0.25	0.02
530	0.03	0.05	0.16	0.01

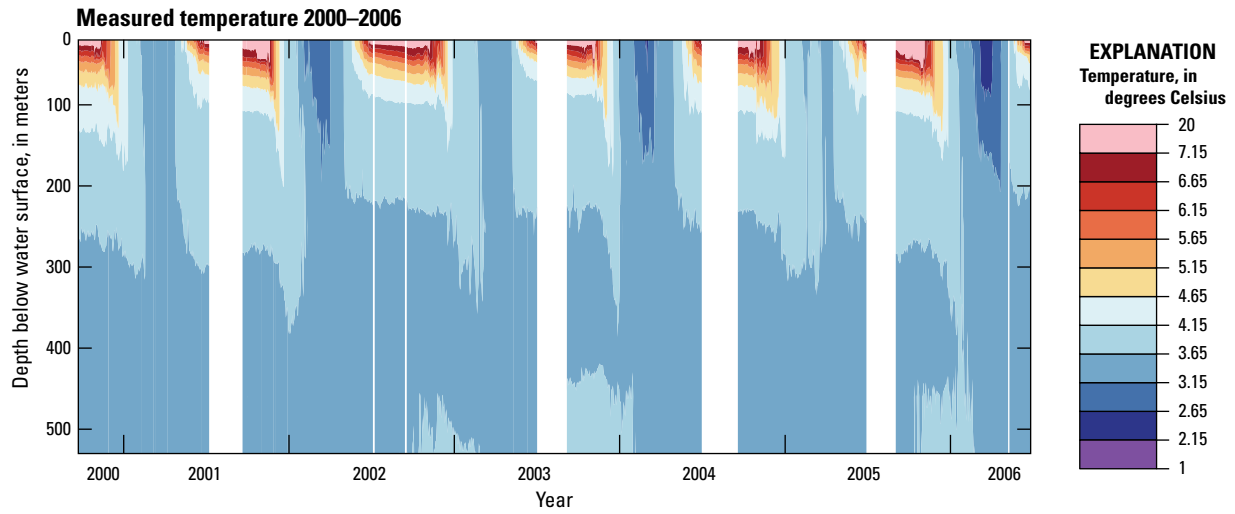


Figure 8. Contour plot showing measured temperature data, Crater Lake, Oregon, 2000–2006.

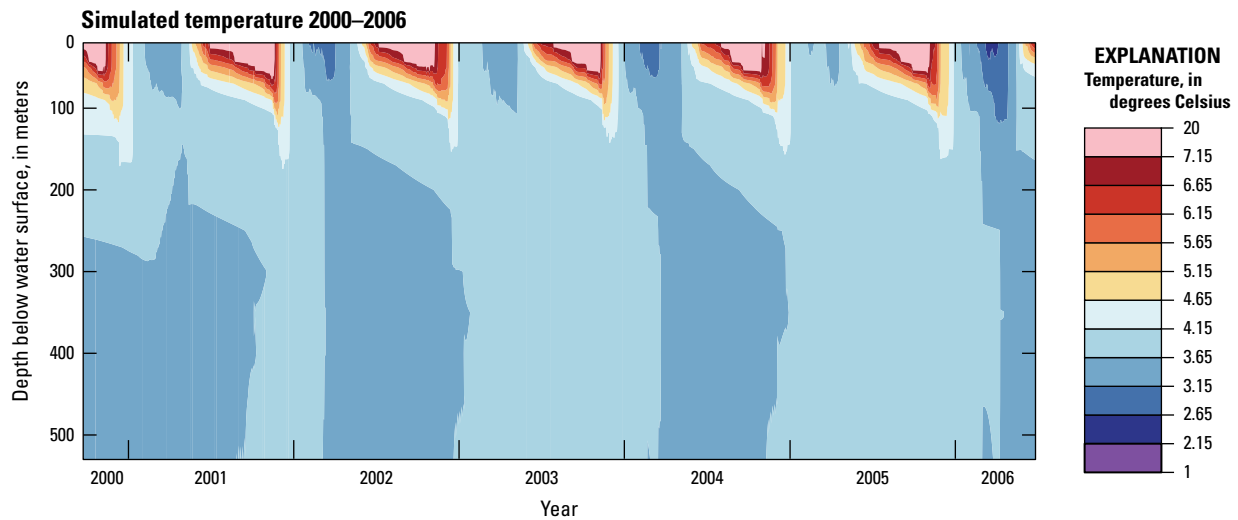
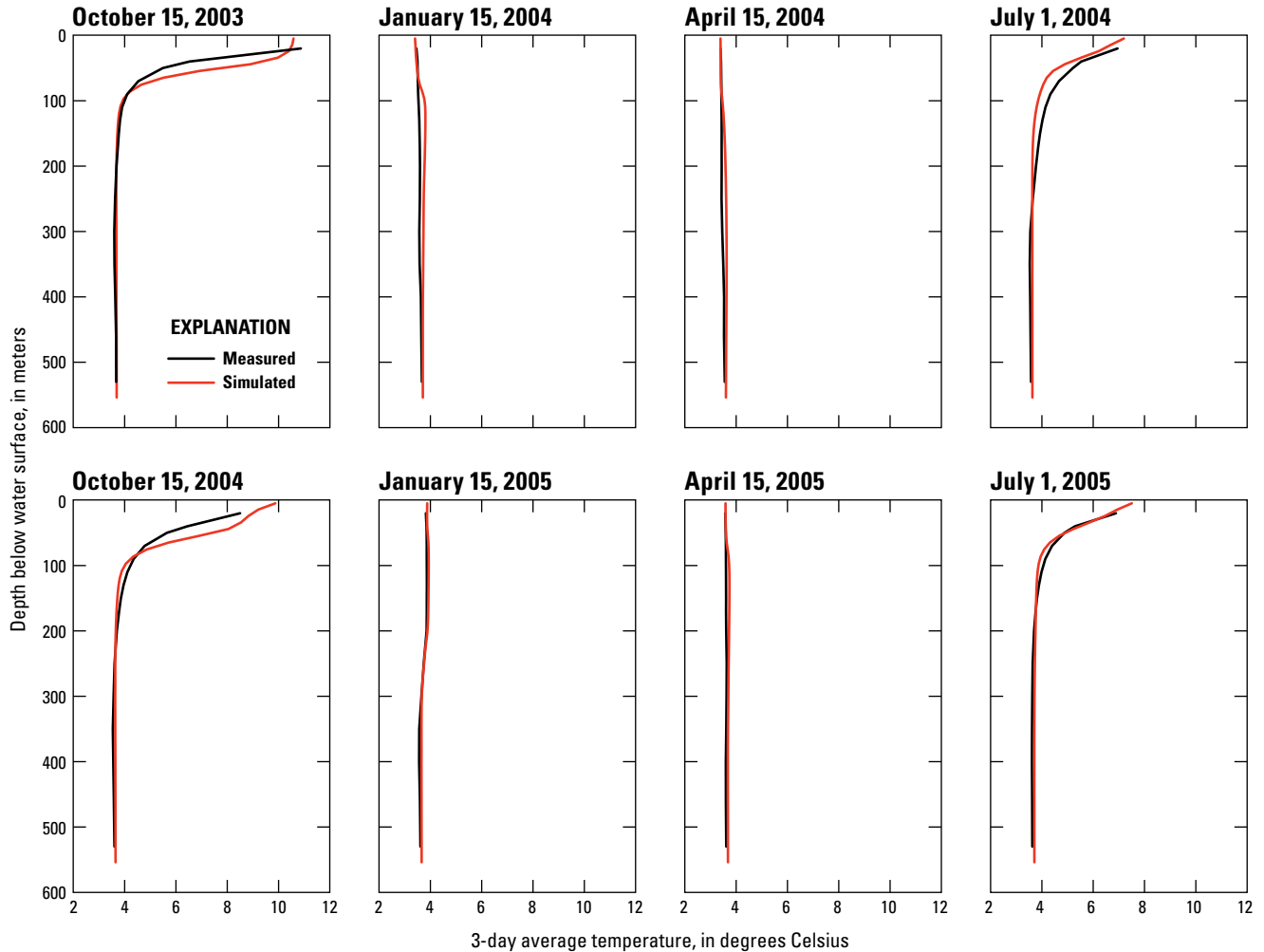


Figure 9. Contour plot showing temperature simulated with the 1-dimensional deep ventilation model, Crater Lake, Oregon, 2000–2006.



**Figure 10.** Comparison of selected measured temperature profiles with profiles simulated with the 1-dimensional deep ventilation model, Crater Lake, Oregon, 2003–2005.

The thermistor data show at least mild cooling in the hypolimnion between 250 and 450 m in most years, even if it does not penetrate to the bottom as in years when a strong ventilation occurs (fig. 11). The simulations do not show such mild cooling every year. The lack of these small adjustments to hypolimnion temperatures can result in a larger simulated event when it does occur, as in 2002. The ability of 1DDV to simulate the small but important variation in temperature at the deep thermistors is quantified by the RMSE normalized by the overall range in measurements (NRMSE), which was largest below 350 m depth (NRMSE between 0.16 and 0.27, table 5).

These features can be seen dynamically in animations of a winter of no deep ventilation (fig. 12) and a winter in which deep ventilation occurred (fig. 13). During the warming phase of the summer, the depth of the simulated thermocline is close to the observed depth in both years. By September, coincident with the cooling phase, the simulated thermocline is too deep and continues to deepen more rapidly than is shown in the observations. In winter, the animations (figs. 12 and 13) show the tendency of the model to underestimate the depth of the mixed layer in winter, starting in February and lasting through April 2003 (fig. 12) and starting in January and lasting through April 2004 (fig. 13).

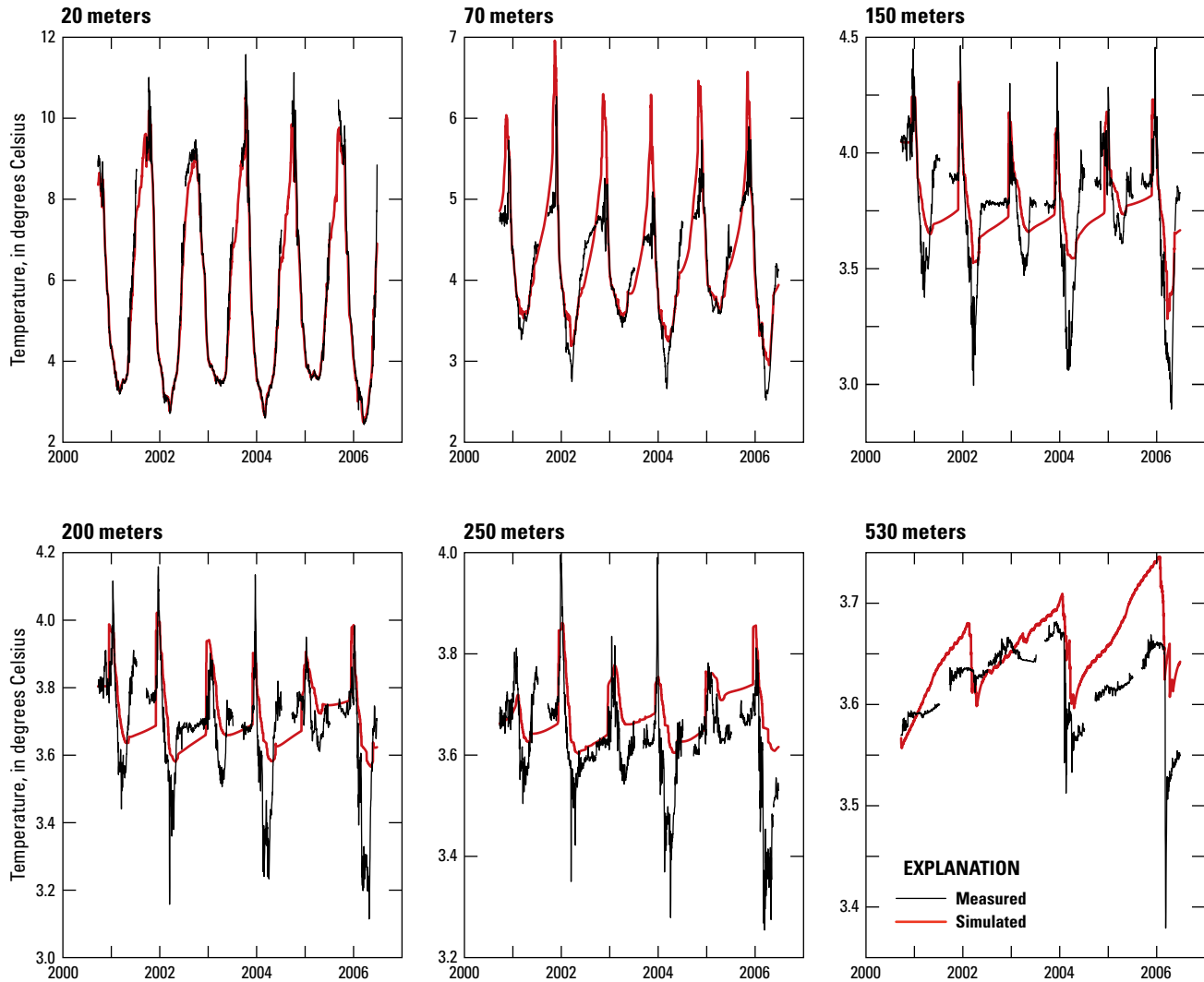


**Figure 11.** Comparison of measured temperature to temperature simulated with the 1-dimensional deep ventilation model at depths between 20 and 530 meters, Crater Lake, Oregon, 2000–2006.

The model, correctly, did not simulate a deep ventilation event in spring 2003 (fig. 12) but it did correctly simulate a deep ventilation event starting in February 2004 (fig. 13). The profile of turbulent diffusivity is relatively dynamic above about 250 m, with a minimum at the thermocline and increasing above to a maximum at the surface. In the hypolimnion, the profile is relatively stable and increases to a maximum in the bottom boundary layer.

For the purposes of this study, more important than accuracy in the simulation of temperature at discrete depths (which was satisfactory) was the ability of the model to simulate the integrated heat content of the upper and lower water column, which is the basis for determining whether deep ventilation occurred in a given year. In Crater Lake,

a natural demarcation between the upper and lower water column occurs at a depth of 325 m because a temperature minimum is usually apparent near this depth in winter temperature profiles, which is the basis for assuming hydrothermal fluxes are confined to greater depths (McManus and others, 1992; McManus and others, 1993), and because thermistors were located at target depths of 300 and 350 m. For the historical period 2000–2006, such events are evident in the lower heat content in the early winter of 2004 and 2006 (fig. 14), and a smaller event is evident in early winter 2002. The ability of 1DDV to simulate the heat content in both the upper water column (above 325 m) and lower water column as calculated from the thermistors was good, as indicated by small overall bias and CVRMSE between 0.01 and 0.05.

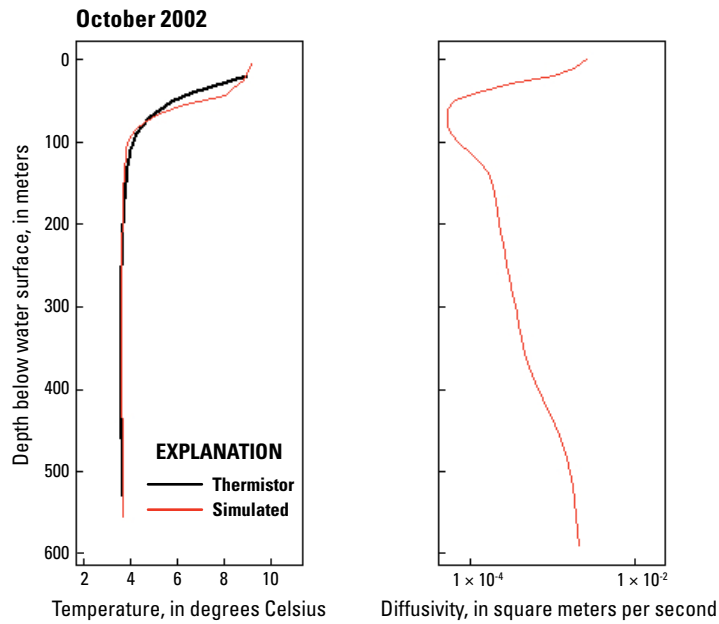


**Figure 12.** Temperature and diffusivity profiles over the autumn to spring months of 2002–2003, when no deep ventilation of the water column occurred, Crater Lake, Oregon. Animation in .AVI format is available for download at <http://dx.doi.org/10.3133/sir20165052>.

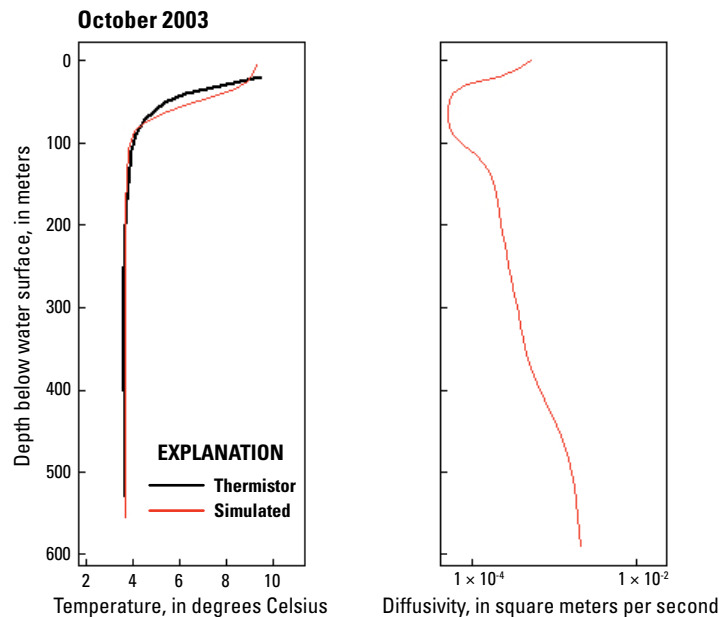


**Figure 13.** Temperature and diffusivity profiles over the autumn to spring months of 2003–2004, when deep ventilation of the water column occurred, Crater Lake, Oregon. Animation in .AVI format is available for download at <http://dx.doi.org/10.3133/sir20165052>.

## 22 Simulation of Deep Ventilation in Crater Lake, Oregon, 1951–2099

The NRMSE values were larger for the lower water column in all three historical periods, between 0.16 and 0.25, as compared to 0.07 to 0.10 for the upper water column (table 6), indicating the challenge of simulating the relatively small

changes in lower water column heat. Most importantly, however, the model correctly simulated the historical series of deep ventilation events, capturing the occurrences in each of 2002, 2004, and 2006 (fig. 14).

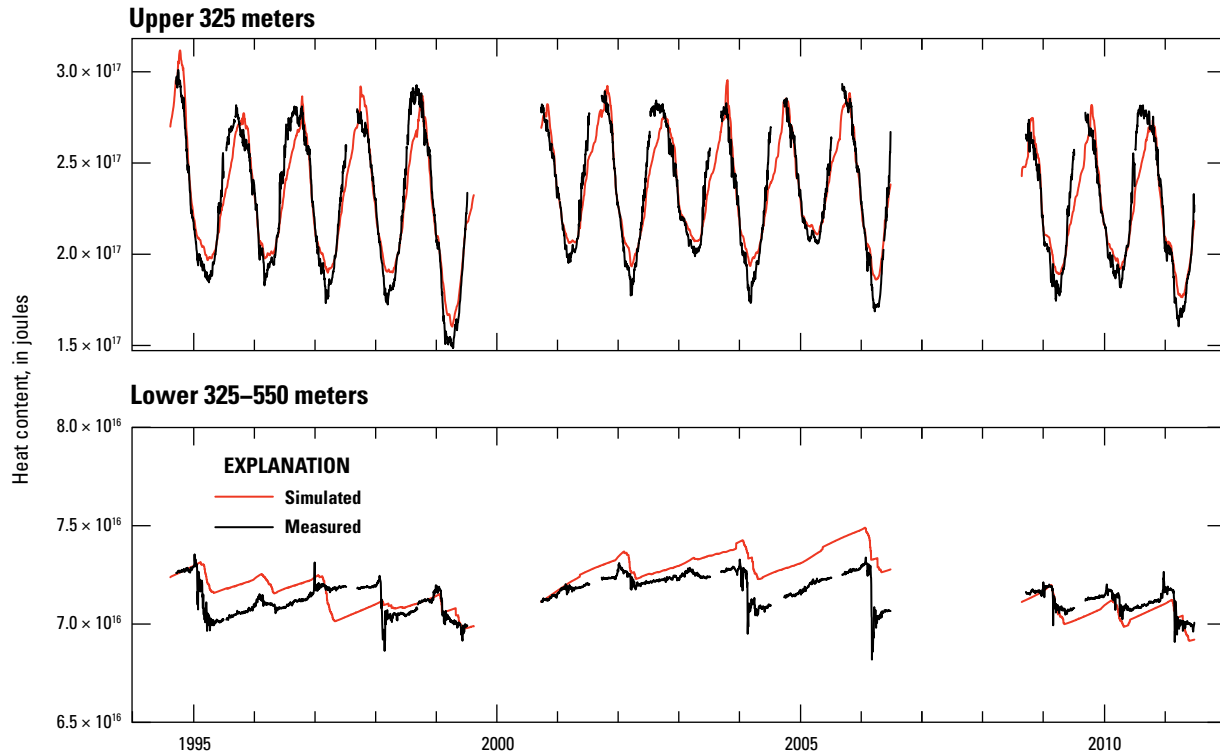


**Figure 14.** Upper and lower water-column heat content calculated from thermistors and from temperatures simulated by the 1-dimensional deep ventilation model of Crater Lake, Oregon, during the calibration years 2000–2006 and the validation years 1994–1999 and 2008–2011.

**Table 6.** Goodness-of-fit statistics for heat content calculated from temperatures simulated by the 1-dimensional deep ventilation model of Crater Lake, Oregon, 1994–2011.

[RMSE: Root-mean-square error. NRMSE: Normalized root-mean-square error (RMSE divided by the range of the observations). CVRMSE: Coefficient of variation of the root-mean-square error (RMSE divided by the mean of the observations). Abbreviations: J, joule; m, meter]

Period	Depth range (m)	Bias ( $\times 10^{15}$ J)	RMSE ( $\times 10^{15}$ J)	NRMSE	CVRMSE
1994–1999	0–325	0.83	11.30	0.07	0.05
	325–550	0.41	1.00	0.21	0.01
2000–2006 (calibration)	0–325	0.73	9.59	0.08	0.04
	325–550	1.10	1.31	0.25	0.02
2008–2011	0–325	0.11	11.80	0.10	0.05
	325–550	-0.42	0.54	0.16	0.01

## Dynamic Reservoir Simulation Model

The hydrothermal fluxes into Crater Lake occur below 350 m depth and have been estimated to be  $1.0 \text{ W/m}^2$  (McManus and others 1992). We modified this value to  $1.4 \text{ W/m}^2$  based on the change in heat content between early and late summer temperature profiles (see section, "Reference Diffusivity Profile") and used this modified value in the DYRESM simulations. (This higher value was confirmed by the simulations done with DYRESM because the flux of  $1.0 \text{ W/m}^2$  was too small to properly capture the warming of deep water when deep ventilation does not occur.) Further definition of the depth distribution of hydrothermal inputs has not been possible, so the total inflow was assumed to be distributed evenly across the sediment area below 350 m depth. To incorporate the diffuse hydrothermal fluxes, the subsurface inflow function of DYRESM was used and it was assumed that the total hydrothermal flux comprised four discrete inflows between 350 and the maximum depth of 592 m (at 375, 425, 475, and 525 m depth). Each of the four discrete inflows integrated the hydrothermal flux of a 50 m depth range centered on the discrete depth. Based on a constant hydrothermal heat flux of  $1.4 \text{ W/m}^2$  and a salinity flux of  $5 \text{ } (\mu\text{g/m}^2)/\text{s}$ , and a total volume of hydrothermal inflow of  $17,280 \text{ m}^3/\text{d}$  ( $140 \text{ L/s}$ ; McManus and others, 1993), the rate of heat input (in joules per day), salt input (in milligrams per day), and hydrothermal inflow (in cubic meters per day) at each of the four depths was calculated based on the fraction of the total bottom surface area included within the range of depths that the discrete source represented. For example, the inflow at 375 m was based on the bottom surface area between 350 and 400 m depth. The calculated temperature and salinity of the hydrothermal inflow applied at the point sources was  $34.73 \text{ }^\circ\text{C}$  and  $0.73$  practical salinity unit (PSU), respectively, based on the total hydrothermal flux of heat and salinity and the total volume of inflow.

## Calibration

The DYRESM parameter suite includes three parameters that control mixing in the upper part of the water column: shear production efficiency ( $\eta_k$ ), potential energy mixing efficiency ( $\eta_p$ ), and wind stirring efficiency ( $\eta_s$ ). Two other parameters influence mixing below the epilimnion: diffusivity at the top of the bottom boundary layer ( $K_{BBL}$ ), and a coefficient of proportionality between eddy diffusivity and lake number ( $C_{LN}$ , our notation). The minimum and maximum layer thicknesses were specified as 2 and 10 m, respectively. Although calibration of the model is not deemed necessary (Imerito, 2014), the model tended toward a deeper-than-observed surface mixed layer in the summer (figs. 15 and 16). Several model runs were made in an attempt to optimize the model parameters for Crater Lake, but substantial quantitative improvement was not obtained, so the DYRESM model was run with default parameter values (table 7) for the mid time period, roughly 8 years from September 1999 to August 2007, using the parameters supplied with the model.

The performance of the model in reproducing the temperature measured at the thermistors was generally good in the upper 100 m of the water column during the winter months, which are most important for this study. In summer, the model reproduced surface temperature well, but over-estimated the temperature at 20 m depth, indicating too much entrainment at the base of the mixed layer (fig. 15). The maximum values of bias, RMSE, and CVRMSE were at 20 m depth ( $0.39 \text{ }^\circ\text{C}$ ,  $1.29 \text{ }^\circ\text{C}$ , and  $0.24$ , respectively; table 8). At the base of and below the seasonal thermocline, between 100 and 200 m, the model simulated the rapid changes in temperature associated with a deepening mixed layer in the cooling phase of the seasonal cycle, but the overall variation in measured temperature was small and the extreme values were not well-captured (fig. 16). In the deep water column, the rapid decreases in temperature of a fraction of a degree associated with deep ventilation events were not well-simulated; indeed, at 530 m there was no change in simulated temperature during the calibration period, indicating no simulated exchange with water from above (fig. 16). Below 350 m, NRMSE varied between 0.30 and 1.52 (table 8).

The ability of DYRESM to simulate the heat content in the upper 325 m as calculated from the thermistors was good, as indicated by the NRMSE and CVRMSE values of 0.10 and 0.05, respectively (table 8), although a summer positive bias is apparent—a result of the thermocline being simulated to be too deep, but also an indication that the input of heat at the water surface was too large. Sensitivity analyses demonstrated that the surface heat budget was sensitive to the cloud cover calculation and the resulting atmospheric longwave radiation calculation (necessary because longwave radiation was not directly measured). The Swinbank (1963) calculation used in DYRESM may not adequately account for the altitude dependence of atmospheric emissivity on atmospheric water vapor (Marty and others, 2002; Ruckstuhl and others, 2007; Yang and others, 2010), resulting in an overestimation of longwave radiation.

As can be inferred from the comparison of model simulation results to the deepest thermistors, DYRESM lacks the ability to simulate the dynamics of the heat content in the lower water column (fig. 17). The NRMSE of 0.32 (table 8) indicates that the simulation of heat content in the lower water column also was quite good, but the statistic does not capture the fact that DYRESM does not simulate the small but important abrupt decreases in lower water-column heat content associated with deep ventilation events, which are clearly seen in figure 17. Thus, DYRESM and 1DDV were both able to simulate temperature and heat content in the upper water column with acceptable accuracy. However, the assumptions on which DYRESM depends are not able to capture the thermobaric instability that is crucial for deep ventilation in the late winter, making this model inappropriate to investigate the phenomenon.

**Table 7.** DYnamic REservoir Simulation Model default parameter values.

[Abbreviations: m, meter; s, second; –, no units]

Parameter	Value	Units
$\eta_k$	0.06	–
$\eta_p$	0.20	–
$\eta_s$	0.40	–
$K_{BBL}$	$1.4 \times 10^{-5}$	m <sup>2</sup> /s
$C_{LN}$	200.00	–

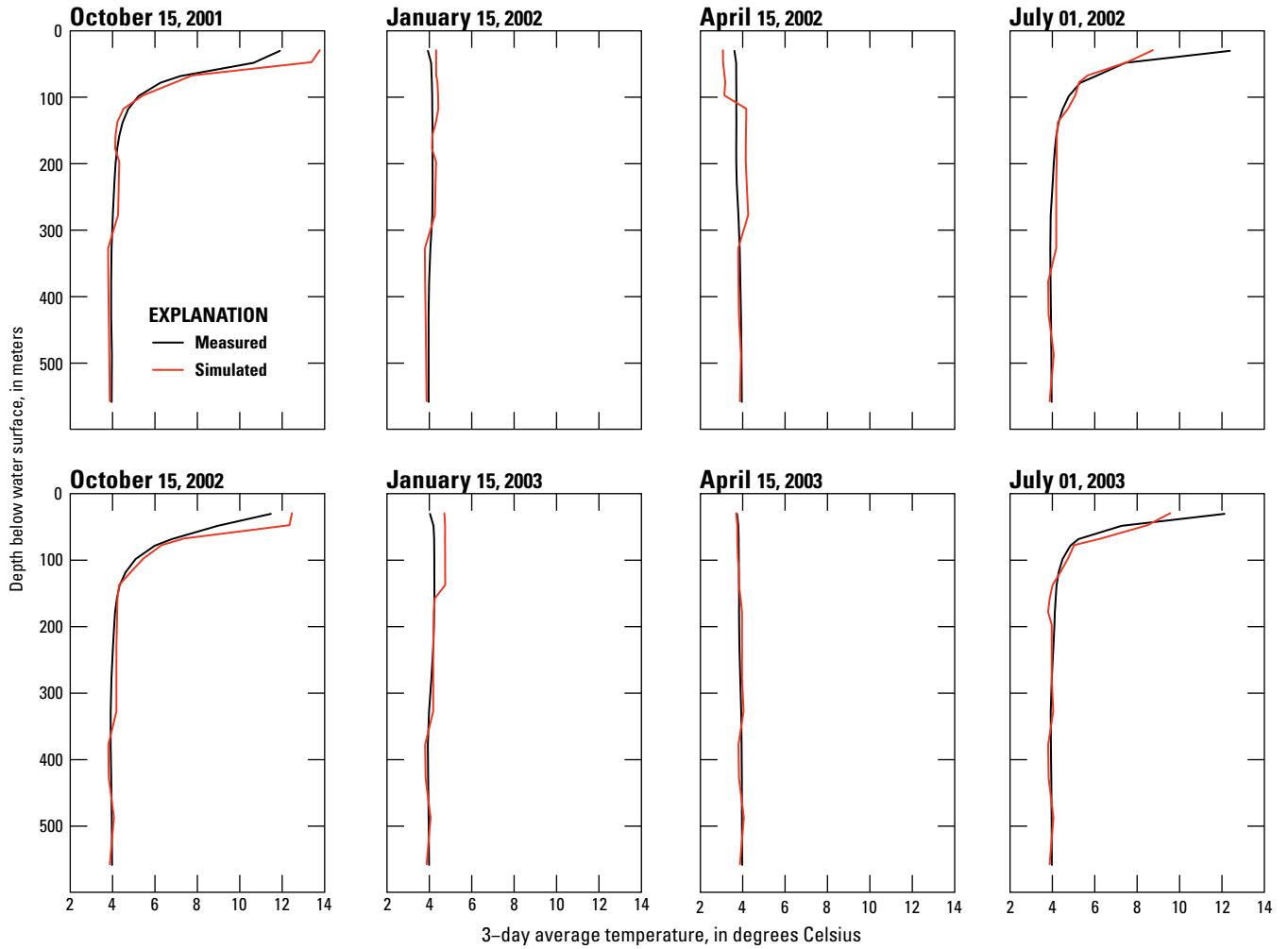
**Table 8.** Goodness of fit statistics for the DYnamic REservoir Simulation Model of Crater Lake, Oregon, 1999–2007.

[RMSE: root-mean-square error. NRMSE: normalized root-mean-square error (RMSE divided by the range of the observations). CVRMSE: coefficient of variation of the root-mean-square error (RMSE divided by the mean of the observations). Abbreviations: m, meter; °C, degrees Celsius; J, joule]

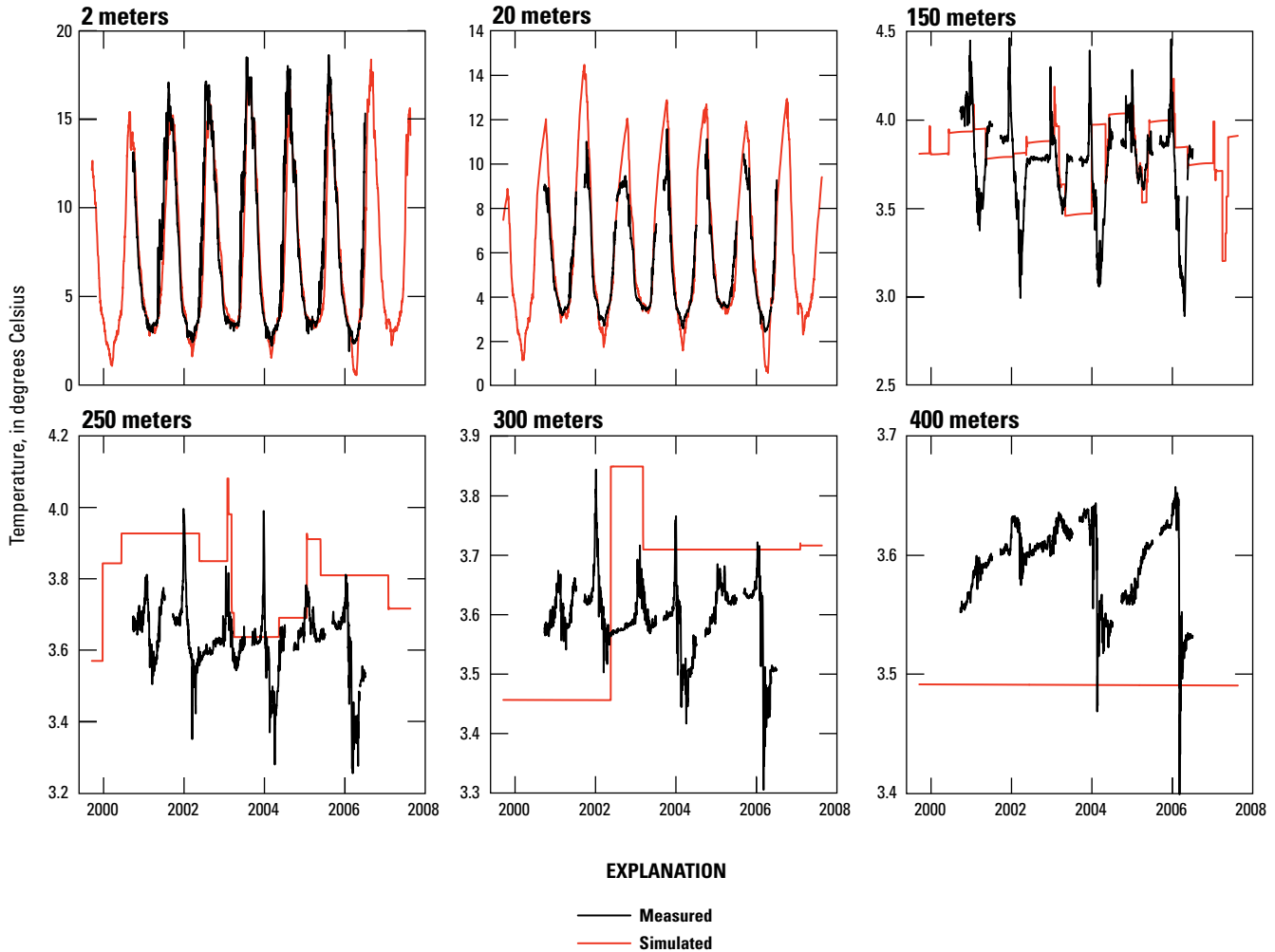
Temperature at thermistor depths				
Depth (m)	Bias (°C)	RMSE (°C)	NRMSE	CVRMSE
20	0.39	1.29	0.14	0.24
40	0.17	0.59	0.10	0.13
50	0.12	0.45	0.09	0.10
70	0.10	0.38	0.10	0.09
90	0.04	0.32	0.11	0.08
110	0.00	0.30	0.13	0.08
130	0.04	0.33	0.17	0.09
150	0.09	0.31	0.20	0.08
170	0.14	0.27	0.20	0.07
200	0.16	0.23	0.22	0.06
250	0.19	0.23	0.31	0.06
300	0.06	0.17	0.32	0.05
350	-0.12	0.12	0.37	0.03
400	-0.10	0.11	0.42	0.03
460	0.16	0.34	1.52	0.09
530	-0.08	0.09	0.30	0.02

Heat content				
Depth range (m)	Bias ( $\times 10^{15}$ J)	RMSE ( $\times 10^{15}$ J)	NRMSE	CVRMSE
0–325	5.16	12.24	0.10	0.05
325–550	0.59	1.66	0.32	0.02



**Figure 15.** Comparison of selected measured temperature profiles to profiles simulated with the DYNAMIC RESERVOIR Simulation Model, Crater Lake, Oregon, 2001–2003.



**Figure 16.** Comparison of measured temperature to temperature simulated with the DYNAMIC RESERVOIR SIMULATION MODEL, Crater Lake, Oregon, 1999–2007.

### One-Dimensional Deep Ventilation Model Validation

Validation focused on the simulation of heat content. Using the selected combination of model parameters, the 1DDV model was run over the two remaining historical periods for which data were available, August 13, 1994, to August 24, 1999 and August 25, 2008, to July 5, 2011. Heat content calculations indicate that the model did a good job of capturing upper lake heat content in both validation periods with an NRMSE less than or equal to 0.10 and CVRMSE equal to 0.05 (table 6). The model performance in simulating heat content in the lower lake was moderately good. For the earlier 1994–1999 period, the heat content calculated from simulated temperature in the lower depths resulted

in an NRMSE of 0.21 (CVRMSE 0.01) when compared to heat content calculated from thermistor data. For the later 2008–2011 period, the heat content calculated from simulated temperature in the lower depths resulted in an RMSE of 0.16 (CVRMSE 0.01). It is noteworthy that the model appropriately simulated deep ventilation in all but 1 year in which it was observed (fig. 14; a strong deep ventilation event was simulated in 1997 when it was not observed, as opposed to 1998 when it was), and the poor correlation from 1994 to 1999 is largely attributable to less-than-observed deep ventilation in 1995, and more-than-observed deep ventilation in 1997. Because the deep lake retains a memory of past years, discrepancies between observed and simulated deep ventilation can propagate. For example, the simulation of more-than-observed deep ventilation in 1997 prevented the

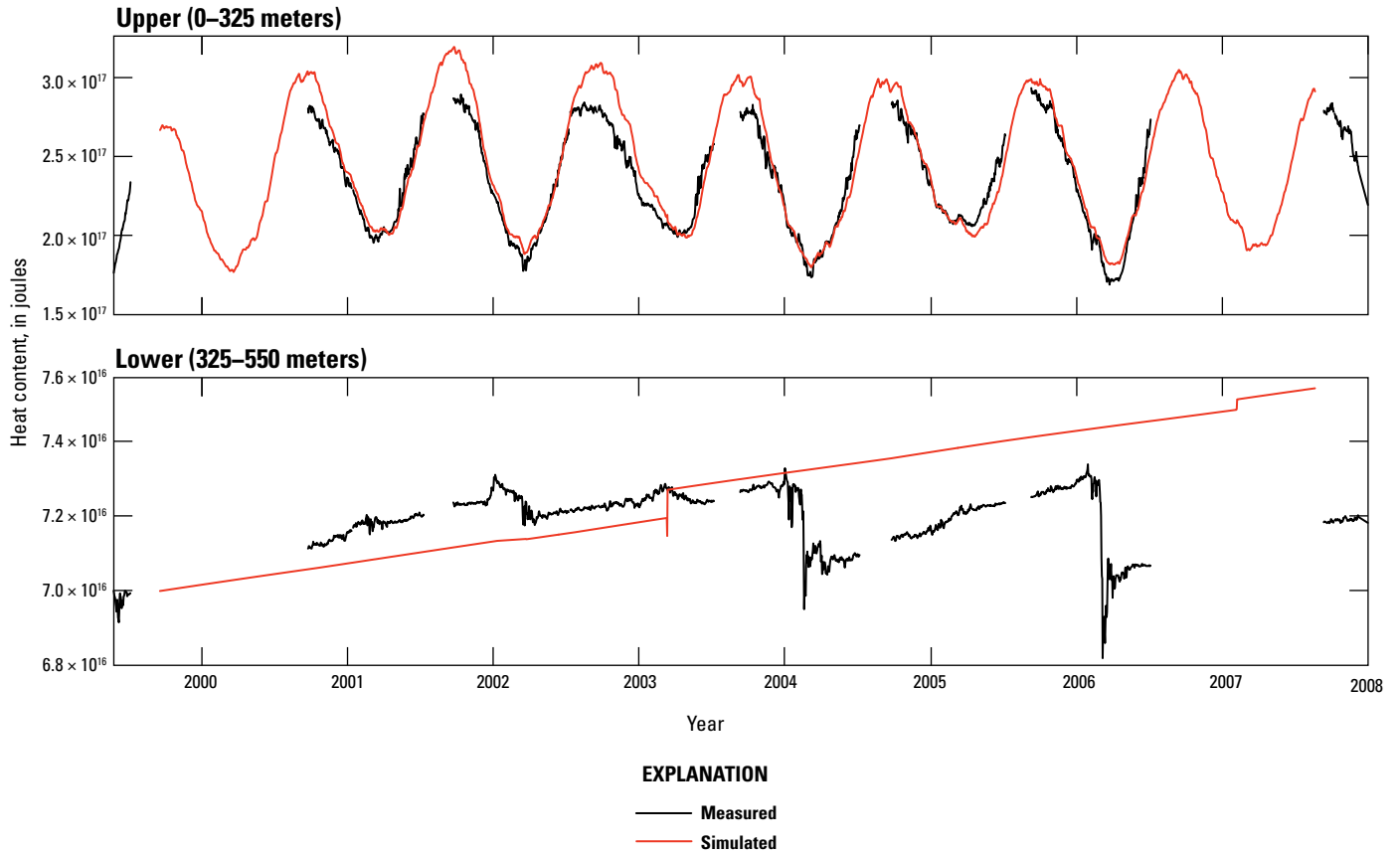


**Figure 17.** Upper and lower water-column heat content calculated from thermistors and from temperatures simulated by the DYNAMIC REservoir Simulation Model of Crater Lake, Oregon, 1999–2007.

simulation of the 1998 event by decreasing the temperature difference between the surface and the bottom at the time when deep ventilation should occur, resulting in a stable temperature profile.

The final validation of the calibrated model was in the form of identifying the occurrence of deep ventilation events. A simple metric used to compare measured thermistor data and simulated values was the difference in lower water column heat content between December and June of each simulation winter–spring season (table 9). There is a significant ( $p=0.03$ ) positive Pearson correlation of 0.34 between the measured and simulated change in lower water column heat content even with the improper simulation of an event in 1997 and resultant lack of a simulated event in 1998 (fig. 18). Most importantly for the purpose of this analysis, the frequency of deep ventilation events was 0.5 for both the measurements and simulations.

**Table 9.** Change in heat content from December to June in the lower water column of Crater Lake, Oregon, 1994–2011.

[Lower water column defined as depths greater than 325 m. Shaded values indicate cooling; bolded values indicate deep mixing events, defined as cooling greater than  $9 \times 10^{14}$  joules. **Abbreviations:** 1DDV, 1-dimensional deep ventilation mode; J, joule; m, meter]

Years	Measured ( $\times 10^{15}$ J)	1DDV simulation ( $\times 10^{15}$ J)
1994–1995	<b>-2.60</b>	<b>-1.16</b>
1995–1996	0.04	-0.48
1996–1997	0.45	<b>-1.97</b>
1997–1998	<b>-1.26</b>	-0.04
1998–1999	<b>-1.53</b>	<b>-1.52</b>
2000–2001	0.42	1.04
2001–2002	-0.25	-0.76
2002–2003	-0.06	0.50
2003–2004	<b>-2.02</b>	<b>-1.37</b>
2004–2005	0.82	0.99
2005–2006	<b>-2.06</b>	<b>-1.98</b>
2008–2009	<b>-0.99</b>	<b>-1.46</b>
2009–2010	-0.57	-0.67
2010–2011	<b>-0.99</b>	<b>-1.75</b>

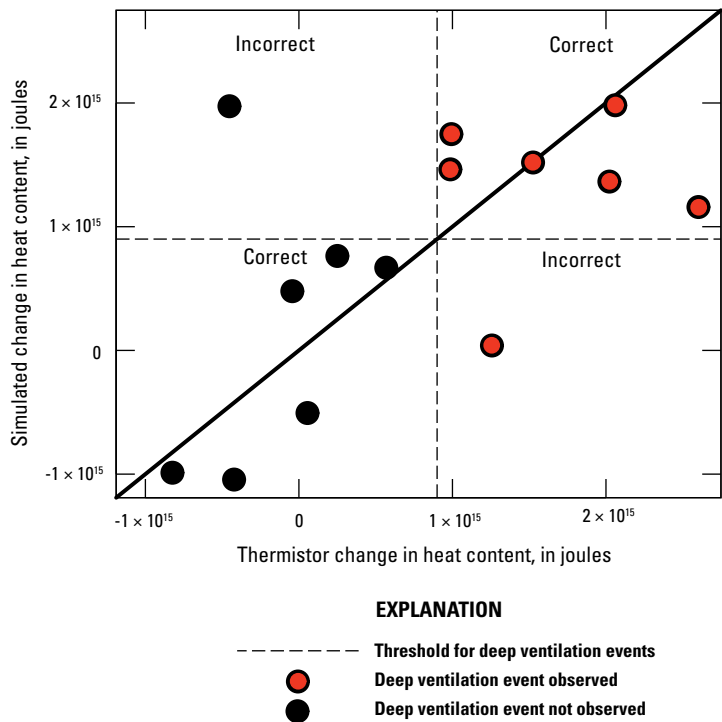


**Figure 18.** Comparison of the change in heat content between December and June as calculated from thermistor data and as simulated with the 1-dimensional deep ventilation model of Crater Lake, Oregon, 1994–1999, 2000–2006, and 2008–2010. Dashed lines represent the  $9 \times 10^{14}$  joule threshold for the change in heat content used to identify deep ventilation events. Quadrants indicate which years were correctly and incorrectly simulated by the 1-dimensional deep ventilation model.

## Results of Future Climate Scenarios

The CNRM-CM5 model projected the mildest air temperature scenario of the three GCMs considered, and this translated to the mildest scenario in terms of the changes to water-column stratification and the frequency of deep ventilation (fig. 19A–B; table 10). Over the 149 years of simulation, spanning the baseline period through 2099, the RCP4.5 scenario projected a transition from deep-water temperatures in the range of 3.3 to 3.8 °C during the baseline period (1951–2005) to a range of 3.5 to 4.3 °C between 2050 and 2099, and a deepening of the 4.3 °C isotherm (fig. 19A). The minimum compensation depth characterizing days when deep ventilation occurred in each year progressively shallowed as an effect of the progressive warming of the entire water column profile, which was caused by increasing surface temperatures. As the entire profile warmed and shifted farther away from the temperature of maximum density curve, the

minimum compensation depth decreased from as deep as 250 m early in the baseline period to no deeper than 50 m after 2070, until the point when the entire water column was always greater than 4 °C and the compensation depth could no longer be defined. After 2050, there was no compensation depth in most years, because temperature in the surface mixed layer did not go below 4 °C (table 1; fig. 20A–B). The RCP8.5 scenario projected water column temperatures greater than 4.3 °C throughout the water column after 2080 and no years of minimum surface mixed layer temperature below 4 °C after 2065 (figs. 19B and 20B).

The most extreme projections came from the HadGEM2-ES model (figs. 19E–F). Over the 149 years of simulation, the RCP4.5 scenario projected a transition from deep-water temperatures in the range of 3.3 to 3.8 °C during the baseline period to a range of 3.8 to greater than 4.3 °C between 2050 and 2099, and a deepening of the 4.3 °C isotherm (fig. 19E). The temperature in the surface mixed layer was less than 4 °C in only 1 year after 2070. The RCP8.5 scenario projected water column temperatures greater than 4.3 °C throughout the water column after 2060 and no years of minimum surface mixed layer temperature less than 4 °C after 2045 (figs. 19 and 20E–F). The HadGEM2-ES RCP8.5 temperature projections lead the CNRM-CM5 RCP8.5 projections by about 20 years.

Once the surface water no longer decreases to below 4 °C in winter, there is no mechanism for thermobaric instability and the vertical extent of mixing is limited to the depth to which convective mixing can penetrate from the surface. Convective mixing to great depth can still occur when the surface water gets colder than the rest of the water column and deep waters have had enough time to warm from hydrothermal inputs; however, this occurs less frequently in future simulations. Such events are evidenced in figure 19 by the appearance of vertical profiles of cooler water between 4 and 4.3 °C. The model shows such deep convective mixing events occurring infrequently after 2070, but they are evident in the RCP8.5 scenarios in 2078 (CNRM-CM5), 2086 (HadGEM2-CC), and 2050 (HadGEM2-ES) (figs. 19B, D, F; figs. 20B, D, F).

The frequency of deep ventilation during the baseline period and in alternative future climates is quantified in table 11. CNRM-CM5 is again the model that projected the most moderate changes of the three GCMs considered. Based on a threshold for change in lower water-column heat content of  $-9 \times 10^{14}$  J, the projected change in the frequency of deep ventilation under the RCP4.5 scenario went from 33 percent during the baseline period to 31 percent in the future conditions. Under the RCP8.5 scenario the projection was a change in frequency from 33 percent during the baseline period to 33 percent in the first 55 years of future conditions, to 18 percent in the second 55 years.

**Table 10.** Linear regression models of upper and lower water-column heat content in Crater Lake, as calculated from temperatures simulated by the 1-dimensional deep ventilation model, for baseline and future conditions from three general circulation models and two representative concentration pathways.

[Change in air temperature: Calculated based on the long-term trend over the entire 93 years of future climate (fig. 4). RMSE: Root-mean-square error. Change in water temperature: Calculated based on the linear trend in the rate of change in heat content for the upper and lower water column, respectively. Abbreviations: m, meter; °C, degree Celsius; J, joule; W/m<sup>2</sup>, watt per square meter]

General circulation model	Upper water column (0–325 m)					Lower water column (325–590 m)					
	Change in air temperature (°C)	Mean daily heat content (×10 <sup>17</sup> J)	Rate of change in heat content		Change in water temperature (°C)	Mean daily heat content (×10 <sup>16</sup> J)	Rate of change in heat content		Change in water temperature (°C)		
			Linear trend (×10 <sup>17</sup> J/decade)	Normalized by area (W/m <sup>2</sup> )			Linear trend (×10 <sup>16</sup> J/decade)	Normalized by area (W/m <sup>2</sup> )		RMSE (×10 <sup>17</sup> J)	RMSE (×10 <sup>16</sup> J)
Baseline conditions: 1951–2005											
CNRM-CM5	1.38	2.29	0.034	0.26	0.329	0.32	7.25	0.009	0.02	0.16	0.02
HadGEM2-CC	0.19	2.37	0.008	0.06	0.323	0.07	7.26	-0.007	-0.01	0.15	-0.02
HadGEM2-ES	-0.30	2.33	0.020	0.15	0.321	0.19	7.19	0.035	0.06	0.16	0.09
First 55 years of future conditions: 2006–2061, representative concentration pathway 4.5											
CNRM-CM5	1.17	2.56	0.036	0.27	0.327	0.34	7.66	0.053	0.09	0.29	0.14
HadGEM2-CC	1.68	2.61	0.084	0.63	0.335	0.80	7.69	0.174	0.30	0.21	0.46
HadGEM2-ES	1.44	2.65	0.076	0.57	0.333	0.73	7.79	0.101	0.17	0.27	0.27
Last 55 years of future conditions: 2045–2099, representative concentration pathway 4.5											
CNRM-CM5	1.17	2.77	0.062	0.47	0.358	0.60	7.97	0.088	0.15	0.35	0.23
HadGEM2-CC	1.68	2.91	0.072	0.54	0.366	0.69	8.36	0.183	0.31	0.39	0.48
HadGEM2-ES	1.44	2.97	0.072	0.54	0.368	0.68	8.42	0.158	0.27	0.34	0.42
First 55 years of future conditions: 2006–2061, representative concentration pathway 8.5											
CNRM-CM5	3.31	2.60	0.072	0.54	0.338	0.68	7.73	0.127	0.22	0.31	0.33
HadGEM2-CC	3.01	2.73	0.124	0.93	0.366	1.18	7.84	0.212	0.36	0.31	0.56
HadGEM2-ES	3.01	2.76	0.142	1.07	0.339	1.36	8.07	0.335	0.57	0.32	0.88
Last 55 years of future conditions: 2045–2099, representative concentration pathway 8.5											
CNRM-CM5	3.31	3.22	0.238	1.79	0.395	2.28	8.84	0.445	0.76	0.44	1.17
HadGEM2-CC	3.01	3.37	0.193	1.45	0.408	1.84	9.36	0.463	0.79	0.65	1.22
HadGEM2-ES	3.01	3.45	0.192	1.44	0.363	1.83	9.98	0.600	1.02	0.37	1.58

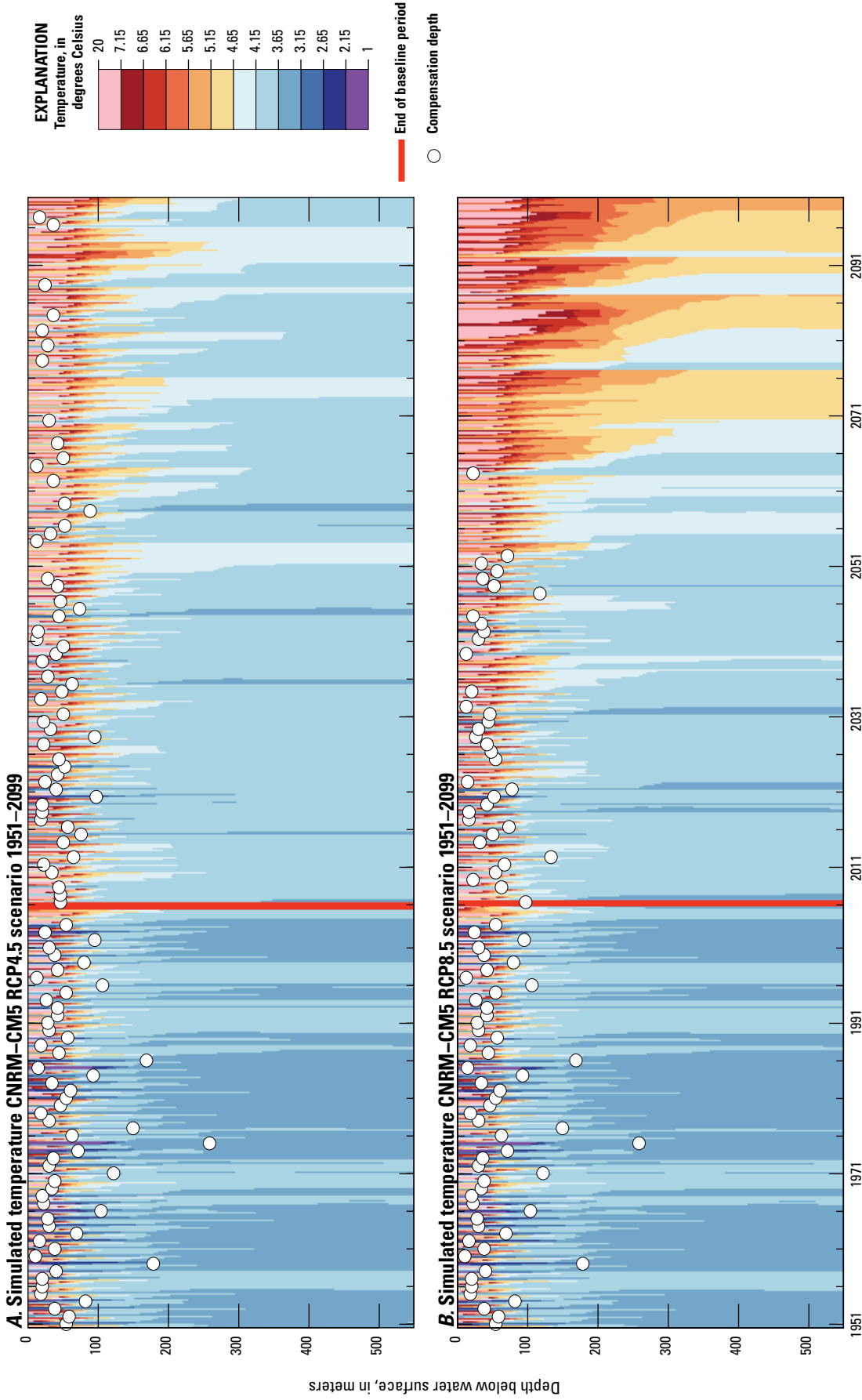


**Figure 19.** Temperature of Crater Lake, Oregon, simulated with the 1-dimensional deep ventilation model, for baseline and future conditions from three general circulation models and two representative concentration pathways. (A) CNRM-CM5, RCP4.5; (B) HadGEM2-CC, RCP4.5; (C) HadGEM2-ES, RCP4.5; (D) HadGEM2-CC, RCP8.5; (E) HadGEM2-ES, RCP8.5; (F) HadGEM2-ES, RCP8.5.

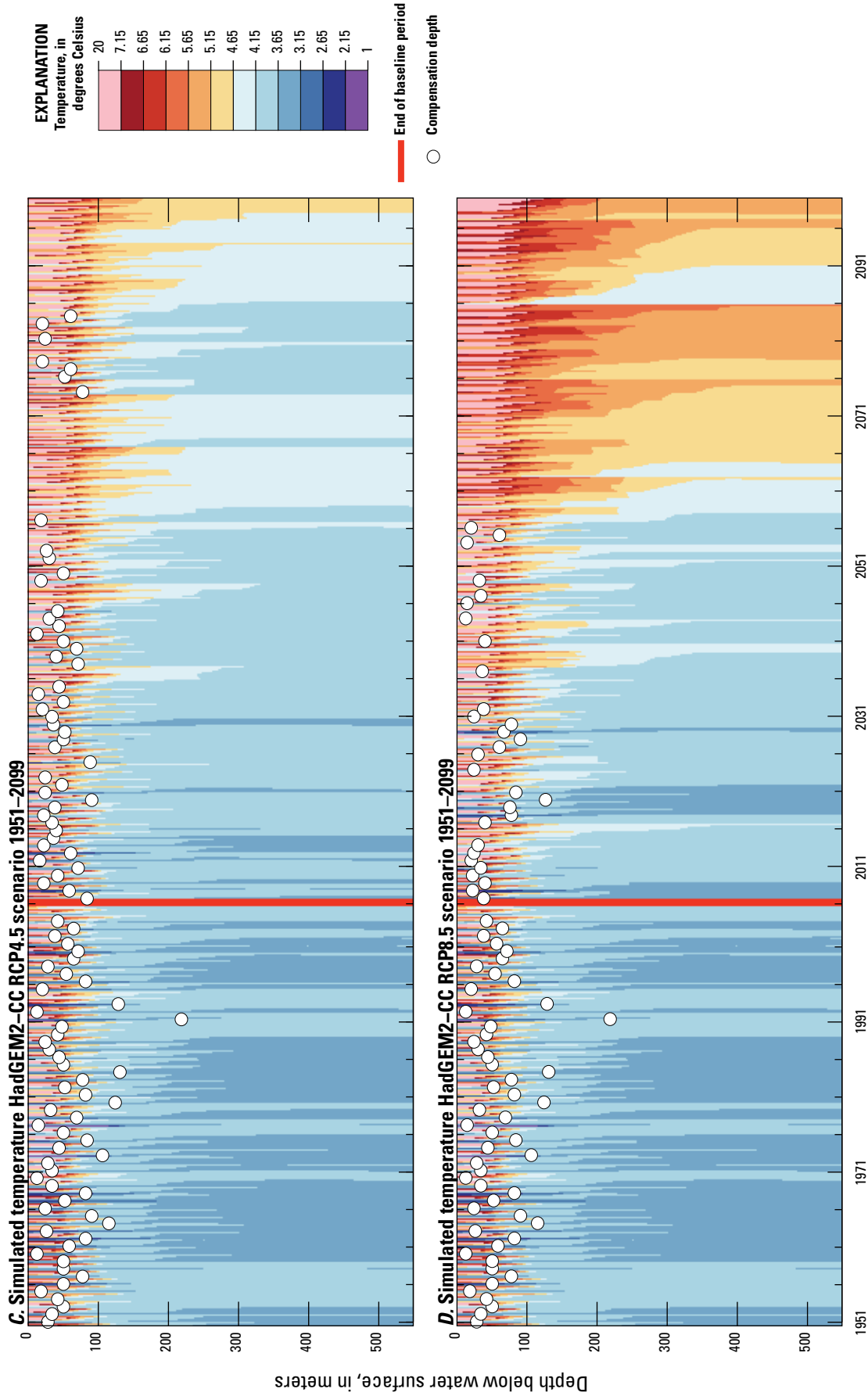


Figure 19.—Continued

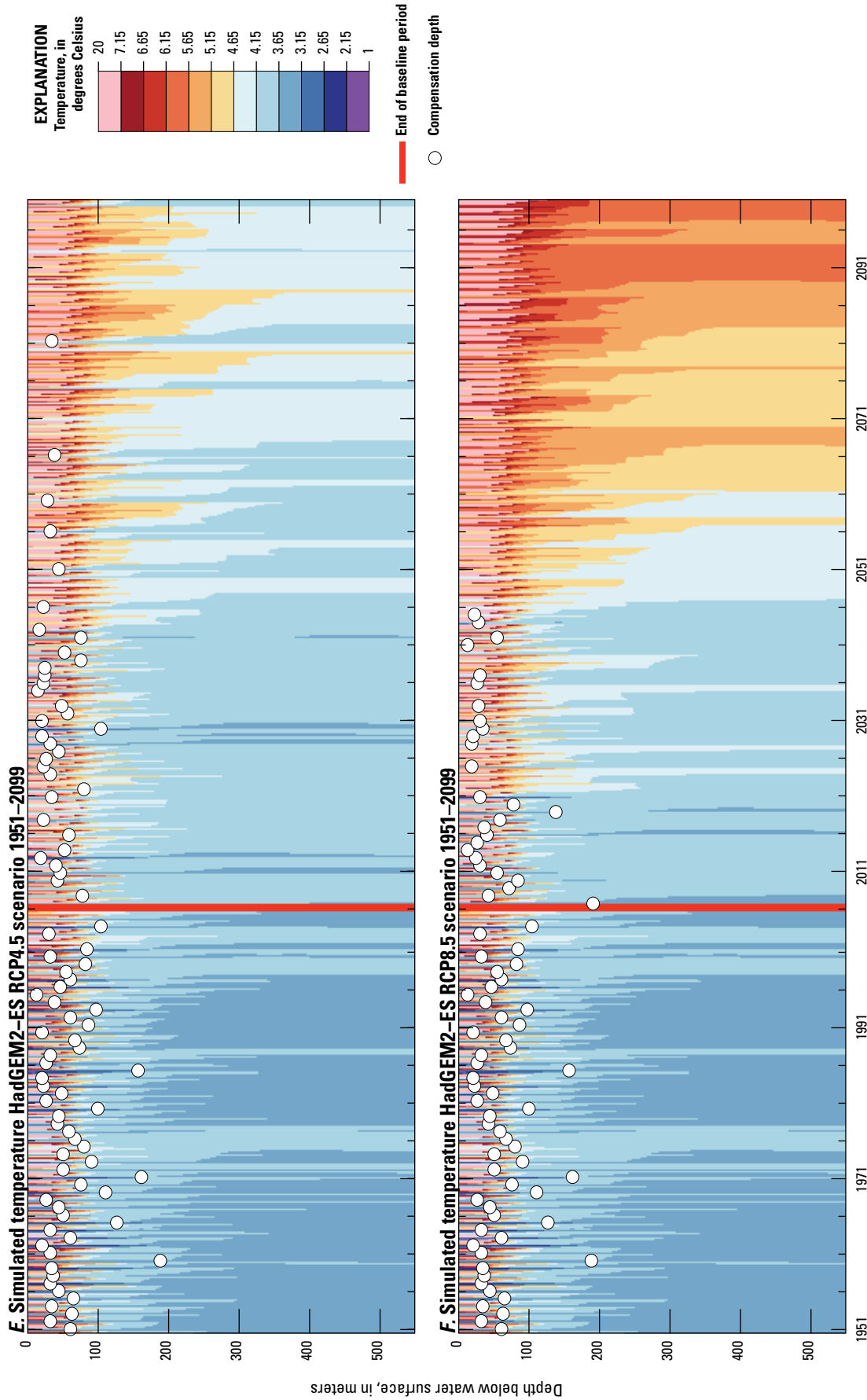
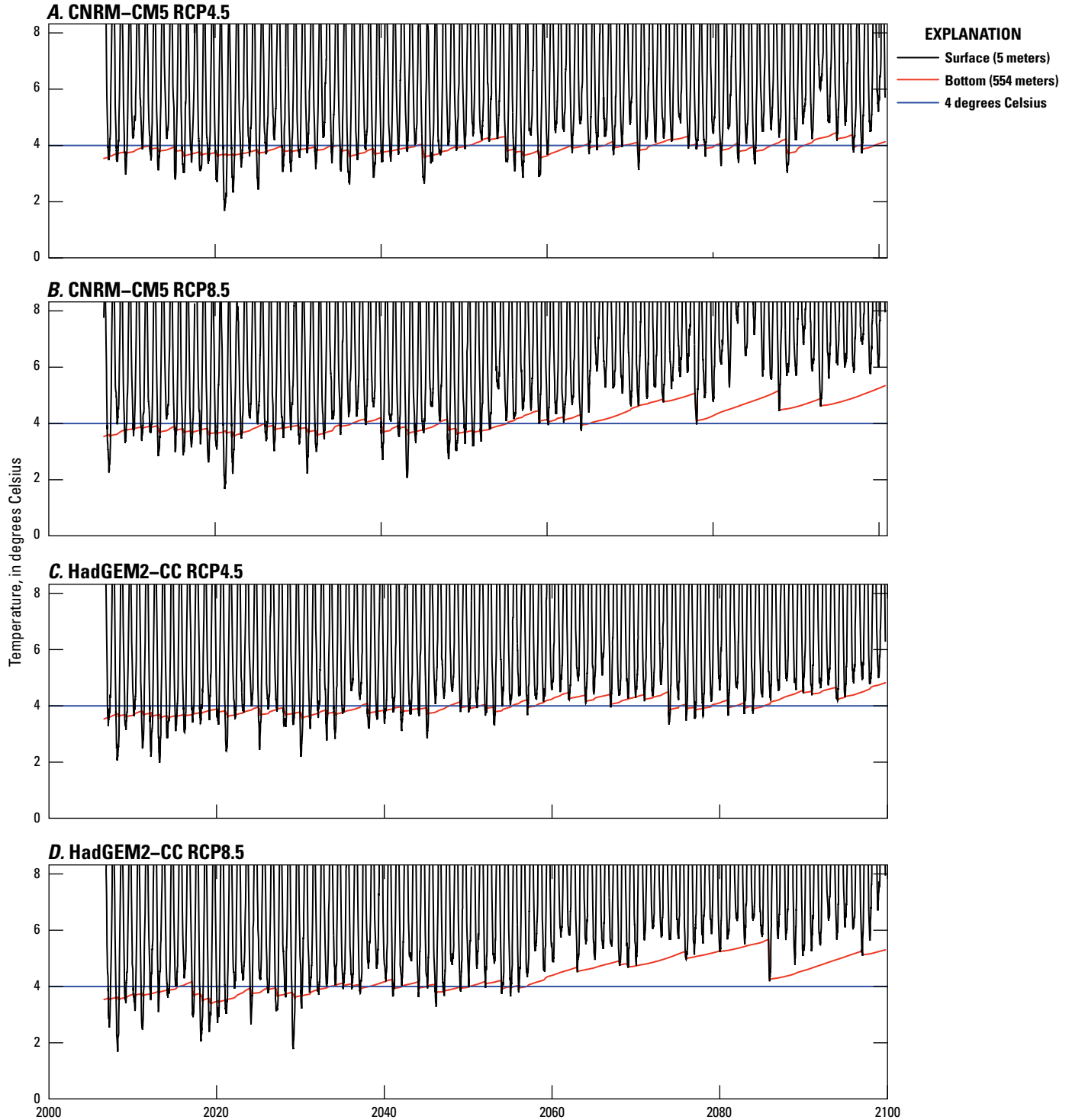


Figure 19.—Continued



**Figure 20.** Surface and bottom temperatures of Crater Lake, Oregon, simulated with the 1-dimensional deep ventilation model, for baseline and future conditions from three general circulation models and two representative concentration pathways. (A) CNRM-CM5, RCP4.5; (B) CNRM-CM5, RCP8.5; (C) HadGEM2-CC, RCP4.5; (D) HadGEM2-CC, RCP8.5; (E) HadGEM2-ES, RCP4.5; (F) HadGEM2-ES, RCP8.5.

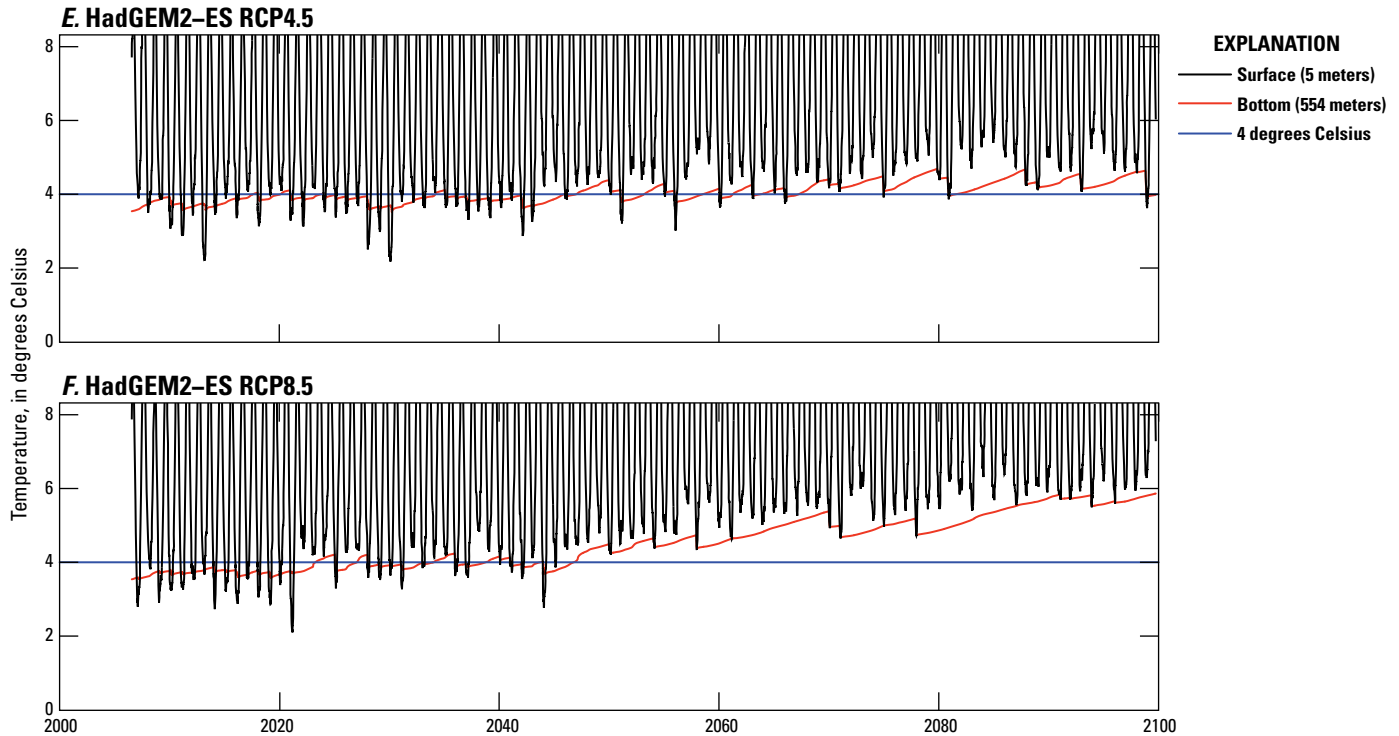


Figure 20.—Continued

The most extreme changes were projected by the HadGEM2-ES model, which projected a change in the frequency of deep ventilation under the RCP4.5 scenario from 55 percent during the baseline period (the closest to that observed during the historical period) to 36 percent in the first 55 years of future conditions, to 25 percent in the second 55 years. Under the RCP8.5 scenario the projection was a change in frequency from 55 percent during the baseline period to 31 percent in the first 55 years of future conditions, to 13 percent in the second 55 years. Based on a threshold for change in lower water-column heat content of  $-9 \times 10^{14}$  J, the HadGEM2-CC GCM simulated a frequency of 44 percent during the baseline period. This GCM projected a change in frequency from 44 percent during the baseline period to 33 percent in RCP4.5 future conditions for all years, and a decrease in frequency to 27 percent in the first 55 years and to 18 percent in the second 55 years of the RCP8.5 scenario future conditions.

Another way to evaluate mixing is in terms of the volume replaced during ventilation events. When the replaced volume was averaged over decades, it was essentially unchanged under future conditions projected by all GCMs in the RCP4.5 scenario (table 12). The CNRM-CM5 and HadGEM2-CC models simulated that the replaced volume actually increased by about 20 percent in the last 55 years of the RCP4.5 scenario.

Previous estimates of the age of deep water have been 2–4 years based on dissolved-oxygen concentration (McManus and others, 1993), 1–2 years based on tritium (Simpson, 1970), and 3.2 years based on chlorofluorocarbons (Weiss, 1992). In our simulations, residence time in the deep lake stayed nearly the same or slightly decreased between baseline conditions and the last 55 years of the RCP4.5 scenario (from 2.52 to 2.14 years, HadGEM2-CC GCM). Projected changes under the RCP8.5 scenario were substantial and all models predicted residence times doubling between the baseline conditions, which ranged 1.88 to 2.90 years, and the last 55 years of the RCP8.5 scenario, which ranged 4.02 to 4.32 years. These changes in the average age of the deep water underscore the fact that the expected changes in a future climate are important in terms of both the frequency of mixing events and the total volume mixed over time.

The upper (0–325 m depth) and lower (325–550 m depth) water column (UWC and LWC) heat content were relatively stable over the 55-year baseline period, and increased most rapidly in the last 50 years of each future climate simulation (fig. 21). The annual and interannual variability in the UWC heat content remained relatively stable through 100 years of future climate, whereas the interannual variability in the LWC heat content increased markedly in future climate scenarios.

**Table 11.** Frequency of deep ventilation during the historical measurement period and during the baseline and future conditions periods from three general circulation models and two representative concentration pathways, Crater Lake, Oregon.

[**Frequency:** Based on a threshold of  $-9 \times 10^{14}$  J for the change in lower water-column heat content between December 1 and June 1 of each winter-spring season. **Mean:** Mean decrease in heat content in a deep ventilation year. **Abbreviations:** 1DDV, 1-dimensional deep ventilation model; J, joule]

Time series	Frequency	Mean ( $\times 10^{15}$ J)
Historical period of observations: 1995–1999, 2001–2006, 2009–2011		
Measured	0.50	-1.64
Simulated with 1DDV	0.50	-1.60
Baseline conditions: 1951–2005		
CNRM-CM5	0.33	-2.21
HadGEM2-CC	0.44	-1.95
HadGEM2-ES	0.55	-1.88
First 55 years of future conditions: 2006–2061, representative concentration pathway 4.5		
CNRM-CM5	0.31	-3.47
HadGEM2-CC	0.33	-3.05
HadGEM2-ES	0.36	-3.53
Last 55 years of future conditions: 2045–2099, representative concentration pathway 4.5		
CNRM-CM5	0.31	-3.87
HadGEM2-CC	0.33	-2.97
HadGEM2-ES	0.25	-4.22
First 55 years of future conditions: 2006–2061, representative concentration pathway 8.5		
CNRM-CM5	0.33	-3.38
HadGEM2-CC	0.27	-3.67
HadGEM2-ES	0.31	-3.65
Last 55 years of future conditions: 2045–2099, representative concentration pathway 8.5		
CNRM-CM5	0.18	-5.28
HadGEM2-CC	0.18	-2.75
HadGEM2-ES	0.13	-5.27

**Table 12.** Replacement volume and residence time in the deep lake, determined during baseline conditions (1951–2005) and future conditions (2045–2099) from three general circulation models and two representative concentration pathways at Crater Lake, Oregon.

[**Volume replaced:** Below 325 meters depth; **Fraction replaced:** Based on a deep lake volume of  $4.98 \text{ km}^3$ ; **Residence time:** Reciprocal of fraction replaced. **Abbreviation:**  $\text{km}^3/\text{yr}$ , cubic kilometer per year]

GCM	Volume replaced ( $\text{km}^3/\text{yr}$ )			Fraction replaced (per year)			Residence time (years)		
	Baseline	RCP4.5	RCP8.5	Baseline	RCP4.5	RCP8.5	Baseline	RCP4.5	RCP8.5
CNRM-CM5	1.72	2.07	1.15	0.34	0.41	0.23	2.90	2.41	4.32
HadGEM2-CC	1.98	2.33	1.24	0.40	0.47	0.25	2.52	2.14	4.02
HadGEM2-ES	2.65	2.55	1.22	0.53	0.51	0.25	1.88	1.95	4.08

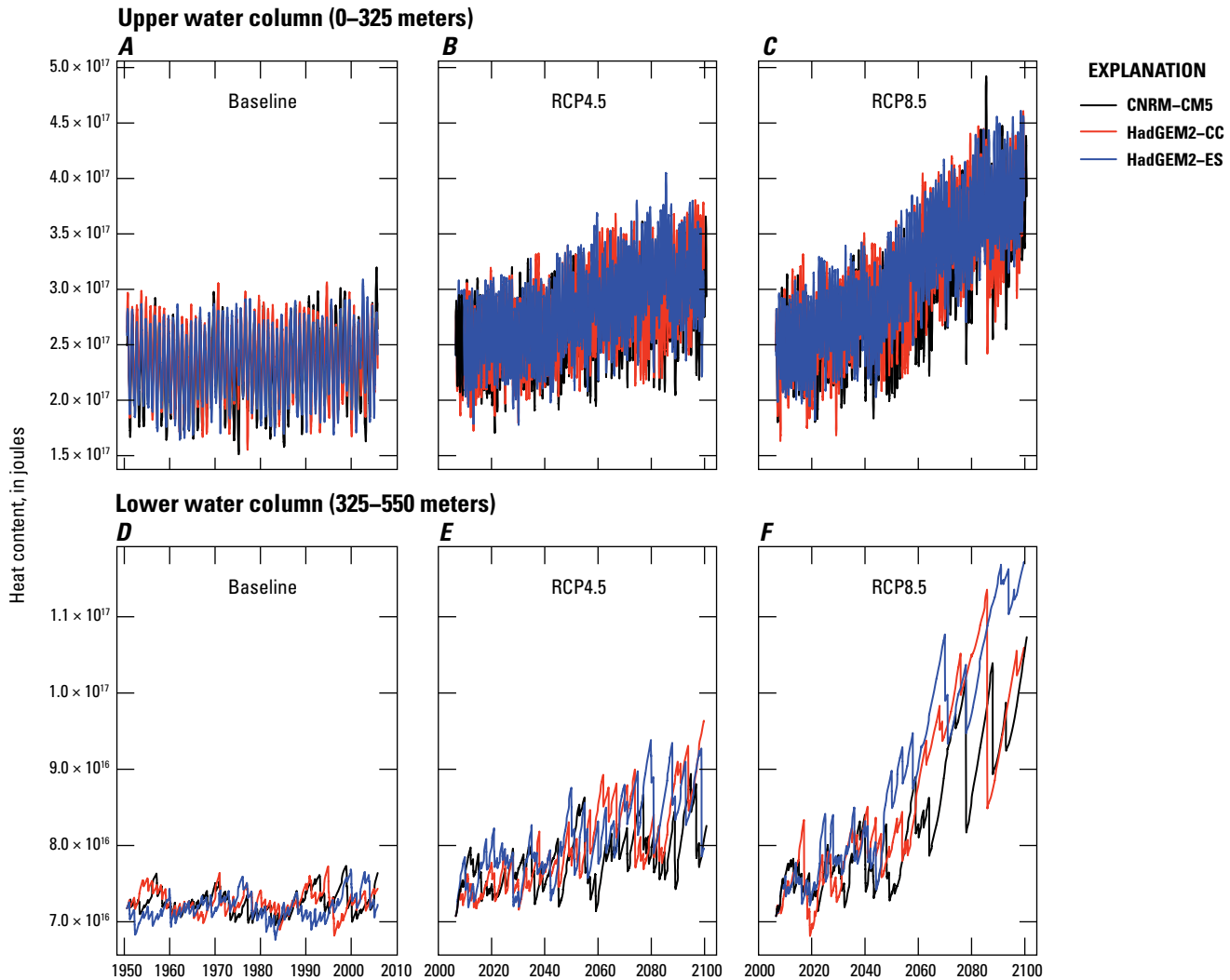


**Figure 21.** Time series showing heat content in Crater Lake, Oregon, as calculated from temperatures simulated by the 1-dimensional deep ventilation model for baseline and future conditions from three general circulation models and two representative concentration pathways. (A) Upper water-column heat content during the baseline period; (B) upper water-column heat content during the period of future climate, RCP4.5 scenario; (C) upper water-column heat content during the period of future climate, RCP8.5 scenario; (D) lower water-column heat content during the baseline period; (E) lower water-column heat content during the period of future climate, RCP4.5 scenario; (F) lower water-column heat content during the period of future climate, RCP8.5 scenario.

Taking the CNRM-CM5 GCM as an example, the UWC heat content increased at a rate of  $3.39 \times 10^{15}$  J (1.5 percent) per decade during the baseline period in response to  $0.025$  °C per year of warming in annual air temperature (table 10, figs. 4A and 21). In the future scenarios, UWC heat content increased  $3.57 \times 10^{15}$  J (1.4 percent) and  $6.23 \times 10^{15}$  J (2.2 percent) per decade in the first and second 55 years of the RCP4.5 scenario, respectively, and  $7.15 \times 10^{15}$  J (2.8 percent) and  $2.38 \times 10^{16}$  J (7.4 percent) per decade in the first and second 55 years of the RCP8.5 scenario, respectively. The RMSE around those slopes was largely consistent, between  $3.29 \times 10^{16}$  J (baseline conditions) and  $3.95 \times 10^{16}$  J (second 55 years of future conditions, RCP8.5). Thus, the interannual and annual variability of the UWC heat content is not much changed in the future scenarios, even as the heat content rises.

In contrast, the LWC heat content, again considering CNRM-CM5 as an example, increased  $5.29 \times 10^{14}$  J (0.69 percent) and  $8.77 \times 10^{14}$  J (1.1 percent) per decade in the first and second 55 years of the RCP4.5 scenario, respectively, and  $1.27 \times 10^{15}$  J (1.6 percent) and  $4.45 \times 10^{15}$  J (5.0 percent) per decade in the first and second 55 years of the RCP8.5 scenario, respectively (table 10). The RMSE around the regression line increased notably between the baseline conditions ( $1.55 \times 10^{15}$  J) and the second 55 years of future climate scenarios ( $3.48 \times 10^{15}$  J or  $4.44 \times 10^{15}$  J), reflecting longer periods between deep ventilation events, and increasingly dramatic decreases in the lower water column heat content when an event occurred (fig. 21). The threshold for thermobaric instability—lake-surface water temperature slightly colder than  $4$  °C—remains the same in

a future climate, but the frequency at which that threshold is met decreases (table 1). Because the heat content in the deep lake continues to steadily increase in response to hydrothermal inputs and the frequency of meeting the surface temperature threshold for deep ventilation caused by thermobaricity decreases, the difference between the deep lake temperature and the 4 °C threshold for deep ventilation becomes greater through time. As a result, the decreases in heat content related to deep ventilation events are less frequent but are larger when they occur. In the last 20 years of the RCP4.5 scenario of the HadGEM2-CC and HadGEM2-ES models, and the last 40–50 years of RCP8.5 scenario for all GCMs, the system warms to the point that the entire water column is greater than the 4 °C threshold (table 1) and thermobaric instability cannot occur. In these periods, the deep ventilation events are convectively driven and only occur when the surface temperatures are less than the deep temperatures, which is infrequent. During these events, the colder surface temperatures are denser than the deep waters and, given sufficient wind energy, are able to mix all the way to the bottom of the lake (figs. 20B, D, F). Thus, the lake is expected to undergo a shift in its thermal regime, progressively transitioning from dimictic to warm monomictic to oligomictic.

The rate of increasing heat content in the UWC and LWC can be compared to the approximately  $1.3 \times 10^{16}$  J per decade of heat (based on  $1.4 \text{ W m}^{-2}$  over the bottom surface area below 350 m) that is put into the deep lake by hydrothermal inflows. The rate of change of heat content in the UWC exceeds this hydrothermal flux only in the second 55 years of the RCP8.5 scenarios (all three GCMs), and in the first 55 years of the RCP8.5 scenarios as projected by the HadGEM2-ES model (table 10). This implies that during baseline conditions and, with one exception, during the first 55 years of future conditions, the lower water column is a source of heat to the upper water column, and the atmosphere is a heat sink for the lake. Only in the second 55 years of the more extreme scenario are air temperatures high enough to overcome the hydrothermal fluxes and turn the atmosphere into a source of heat to the lake.

## Comparisons to Future-Climature Studies of Other Lakes

All of the future climate scenarios that were used to simulate the daily water temperature profile in Crater Lake through the year 2099 projected increased water temperature throughout the water column and a decreased frequency of deep ventilation events. Under the assumption that the realized future conditions will be within the range of outcomes encompassed by the six scenarios used in this study—three GCMs and two representative concentration pathways—the

long-term average temperature in the upper water column (defined to be above 325 m depth) of Crater Lake can be expected to increase between 0.94 and 3.19 °C between 2006 and 2099, and the corresponding increase in the hypolimnion (below 325 m depth) is between 0.37 and 2.46 °C. In the RCP8.5 scenario, all GCMs show the entire water column warming to greater than 4.3 °C year-round after 2080 and in the RCP4.5 scenario, all GCMs show the entire water column warming to greater than 3.5 °C year-round after 2080.

Studies of the effects of climate change on temperate lakes worldwide share several conclusions regarding the expected changes in the epilimnion. First, water temperatures will increase in proportion to air temperature, and, generally, the increase is greater than 50 percent (Peeters and others, 2002; Livingstone, 2003; Hampton and others, 2008) and as much as nearly 100 percent (Coats and others, 2006; Peeters and others, 2007; Perroud and Goyette, 2010) of the increase in air temperature depending on how it is measured—monthly, seasonal, or annual means; a long-term average; daily minimums or daily means. Second, the annual number of days of stratification will increase, and third, annual periods of ice cover will shorten in high-latitude lakes (Robertson and Ragotzkie, 1990; Hostetler and Giorgi, 1995; Elo and others, 1998; Hostetler and Small, 1999). Overall, these and other studies have concluded that in a future climate, the epilimnion of lakes will respond quickly and in direct and high proportion to warmer air temperature and the accompanying changes in other meteorological drivers such as longwave radiation and evaporation.

Conclusions regarding the temperature in the hypolimnion of lakes are less consistent, which is not surprising particularly because the thermal mass per surface area varies with the overall depth of the lake and the climate setting of the lake is important. The hypolimnion in temperate lakes that remain dimictic and reliably inverse stratify in winter are not expected to retain a climate signal or warm in a future climate (Butcher and others, 2015). In monomictic lakes deep enough to establish a seasonal thermocline, the influence of the atmosphere is transmitted to the hypolimnion by means of mixing with the epilimnion outside of the stratified season; therefore, in lakes that reliably mix at least once per year, the hypolimnion receives the climate signal embedded in epilimnion temperatures prior to the onset of stratification and carries it through the stratified season to the next autumn or spring mixing event, resulting in a trend in the annual average hypolimnion temperature that reflects the climate signal rather than seasonal fluctuations (Dokulil and others, 2006). Deep lakes that do not mix every year hold a long-term “memory” of the climate manifested as a slow interannual upward trend in temperature as heat diffuses from above, punctuated periodically by rapid cooling when deep-mixing events occur, resulting in a “sawtooth” pattern in the temperature or heat content (Livingstone, 1997; Ambrosetti and Barbanti, 1999).

**Table 13.** Long-term changes in lower water-column temperature in deep lakes (> 100 m depth), based on historical measurements and modeling studies of future climate scenarios.

[Lower water column: Greater than 325 m depth for Crater Lake, equivalent to the hypolimnion for other lakes. **Abbreviation:** GCM, general circulation model; °C, degrees Celsius; m, meter; ~, approximately; –, no data; na, not applicable]

Lake	Latitude	Elevation (m)	Maximum depth (m)	Lower water column		Air temperature increase (°C)	Calculation of lake temperature	Historical or future period	Reference
				Temperature change (°C)	Temperature change normalized by air temperature change				
Lake temperature changes based on historical observations									
Zurich	47.3°N	406	136	0.28–0.53	0.28–0.53	~1 (in the daily minimum)	Maximum decadal mean increase; range is by season	1947–1998	Livingstone (2003)
Tahoe <sup>1</sup>	39.1°N	1,898	500	0.64	0.85	~0.75 (in the daily minimum)	Long-term trend slope	1970–2002	Coats and others (2006)
Baikal			1,600	–	–	1.20	Long-term trend slope at 25 m depth	1945–2005	Hampton and others (2008)
Lake temperature changes based on modeling studies of future climate									
Geneva	46.4°N	372	309	2.20–2.33	0.53–0.56	4.13	Range in monthly means	na	Perroud and Goyette (2010)
Constance	47.6°N	395	254	2.6–2.9	0.6–0.7	4	Range in monthly means	na	Peeters and others (2007)
Zurich	47.3°N	406	136	1.4	0.35	4	Annual average	na	Peeters and others (2002)
Crater	43.0°N	1,883	590	0.26–0.69	0.13–0.24	2.02–2.91 (range of RCP4.5 scenarios and 3 GCMs, annual means)	Based on trend calculated over first and last 55 years	2006–2099	This study
				1.23–2.04	0.22–0.40	5.20–5.72 (range of RCP8.5 scenarios and 3 GCMs, annual means)	Based on trend calculated over first and last 55 years	2006–2099	

<sup>1</sup>Values are approximate. Water temperature increase based on the slope at 300 m (hypolimnion) in table II of Coats and others (2006). Air temperature increase determined graphically from figure 8 in Coats and others (2006).

It might be reasonable to assume that the climate signal would be more difficult to discern in the hypolimnion of deep lakes with a vast hypolimnetic volume to “dilute” the climate signal from the much smaller epilimnetic volume; however, although it is challenging to compare studies because of the different methods of reporting results, other studies of deep lakes do not necessarily support that assumption (table 13). For example, Coats and others (2006) determined from more than 33 years of historical record that the hypolimnetic temperature increase in Lake Tahoe, United States (500 m maximum depth) was approximately 81 percent of the increase in the epilimnetic temperature in response to an approximately 0.75 °C increase in air temperature. A study of 52 years of record in Lake Zürich, Switzerland (136 m deep) determined that the hypolimnetic temperature increase was between 48 and 61 percent of the epilimnetic temperature increase in response to a similar increase in air temperature (about 1 °C; Livingstone, 2003). Among modeling studies of future climate, all of which considered air temperature increases of about 4 °C, the increase in hypolimnetic temperature was 73 percent of the increase in epilimnetic temperature (annual average) in Lake Zürich (136 m maximum depth; Peeters and others, 2002), between 69 and 87 percent (range in monthly means) in Lake Constance, Germany (254 m maximum depth; Peeters and others, 2007), and between 61 and 95 percent (range in monthly means) in Lake Geneva, Switzerland (309 m maximum depth; Perroud and Goyette, 2010). This small set of studies suggests that, on decadal time scales, the hypolimnion even in the deepest lakes responds to the atmospheric changes at the surface.

By comparison, the projected deep hypolimnetic (below 325 m) temperature increase in Crater Lake is moderate, particularly for the RCP4.5 scenarios. The long-term mean hypolimnetic temperature increase, as a percentage of the air temperature increase, is projected in the range of 13–24 percent (corresponding to an absolute increase between 0.26 and 0.69 °C) across the three GCMs, as compared to Lake Tahoe, a lake of similar depth to Crater Lake, for which the same percentage measured over 33 years of historical record was 85 percent (table 13; Coats and others, 2006). However, the projected increase in temperature shown in table 13 is based on long-term linear trends in heat content calculated over 55-year segments (table 10) and clearly underestimates both the rate of increase and the absolute increase in temperature projected to occur over shorter timeframes between less and less frequent deep ventilation events (fig. 20). For the RCP8.5 scenarios, the projected increase in temperature across the three GCMs is 22–40 percent of the air temperature increase, or 1.23–2.04 °C. Therefore, the projected temperature increase in the hypolimnion, as a percentage of the air temperature increase, is bigger for the larger increase in air temperature projected by the RCP8.5 scenarios. In these scenarios, the lake becomes oligomictic much earlier, and the temperature

in the deep hypolimnion increases in response to the strong hydrothermal heat flux. Thus, the primary effect of the atmospheric changes is not to provide more direct heat transfer to the hypolimnion in the future, but rather to decrease cooling of the hypolimnion. This decrease in cooling is bigger for the RCP8.5 scenario, as indicated by a lower frequency of deep ventilation events.

## Conclusions

The ventilation of the deepest water and cooling of the hypolimnion in Crater Lake is initiated by thermobaric instability. Over long time periods, the largest effect of warmer surface temperatures is on the frequency at which the necessary conditions for thermobaric instability are established. Currently, the reverse stratification that enables deep ventilation events initiated by thermobaric instability occurs in about 50 percent of years. All the future climate scenarios considered show that the number of days during which this condition is met will decrease in the future. The least extreme scenario (CNRM-CM5, RCP4.5) shows this condition occurring nearly every year and on as many as 200 days in a year through 1990, then tapering off until the condition is met in less than 50 percent of years by 2100, usually on less than 100 days in a year. Mostly as a consequence of this change in lake surface temperature, the frequency of deep ventilation events is projected to decrease from about 50 percent in current conditions to 31 percent by 2100. The most extreme scenario considered in this study showed lake surface temperatures never cooling to less than 4 °C after 2050, and projected the frequency of deep ventilation events to be 13 percent by 2100. In these periods, the deep ventilation events are convectively driven and occur infrequently, only when the surface temperature is less than the deep temperature.

The temperature gradient in the deep lake is nearly two orders of magnitude greater than adiabatic and would be unstable but for the hydrothermal inputs of salinity as well as heat (McManus and others, 1993). In this application of 1DDV, salinity was not simulated dynamically; rather, the salinity profile was held fixed at a historical average, and therefore, the stabilizing effect of salinity on density in the hypolimnion was maintained through time. In a future climate in which deep ventilation occurred less frequently, the salt content below approximately 350 m would increase with the increase in heat content as a result of hydrothermal inflows. Simulations in this study, which did not allow salt content to increase in proportion to heat content, probably underestimated the stabilizing effect that salinity would have in the distant future. For this reason, the decreased frequency of deep ventilation of the deep lake in future climates could be greater than what was demonstrated in this study.

The hydrothermal inputs to the lake were estimated at  $1.4 \text{ W/m}^2$ , 40 percent higher than the previous estimate of  $1 \text{ W/m}^2$ . At either value, it is clear that the function of the atmosphere in the long-term heat budget since the caldera filled has been as a heat sink for the lake. This is not projected to change in the future climates considered, until the last 55 years of the RCP8.5 scenario. The hydrothermal inputs imply that the profundal changes in Crater Lake in a future climate could be different from those projected for deep lakes receiving relatively little hydrothermal heat inputs. In the complete absence of cooling, hydrothermal heating at the rate of  $1.4 \text{ W/m}^2$  would increase the temperature of the hypolimnion below 325 m depth by about  $0.39 \text{ }^\circ\text{C}$  per decade, which could be considered the upper limit on the rate of temperature increase. In the event, therefore, that deep ventilation events stop completely in a future climate, the projected lake temperature changes could be underestimates.

## Summary

The frequency of deep ventilation events in Crater Lake, a caldera lake in the Oregon Cascade Mountains, was simulated in six future climate scenarios. The 1-dimensional deep ventilation (1DDV) model used was developed specifically to simulate the ventilation of deep water initiated by reverse stratification and subsequent thermobaric instability, which allows water colder than the temperature of maximum density at the surface to be unstable when displaced downward a sufficient distance by wind action, and to sink to the deep lake. The model, which is forced with wind speed and lake surface-water temperature, was calibrated with lake temperature data collected from 2000 to 2006, and validated with data from 1994 to 1999 and 2008 to 2011. Emphasis in the calibration and validation was placed on the correct simulation of wintertime deep ventilation events, and their frequency. The simulated annual frequency of these events in the calibration/validation of the model was 0.5 (1 in 2 years), as compared to 0.5 in the historical data.

Wind and air temperature data from three general circulation models (GCMs) (CNRM-CM5, HadGEM2-CC, and HadGEM2-ES) and two representative concentration pathways (RCP4.5 and RCP8.5, corresponding to a moderate and more extreme future, respectively) were statistically downscaled using the Multivariate Adaptive Constructed Analogs (MACA) technique, bias corrected using measurements from the surface of Crater Lake, and then used to simulate the change in lake temperature and the frequency of deep ventilation events in possible future climates. The lumped model *air2water* was used to project lake surface temperature, a required boundary condition for the lake model, based on air temperature in the future climates.

The 1DDV model was used to simulate daily water temperature profiles for 55 years of baseline conditions and 95 years of future conditions for all six combinations

of GCMs and RCPs. All future climate scenarios projected increased water temperature throughout the water column and a substantive reduction in the frequency of deep ventilation events. The least extreme scenario (CNRM-CM5, RCP4.5) projected the frequency of deep ventilation events to decrease from about 1 in 2 years in current conditions to about 1 in 3 years by 2100. The most extreme scenario considered (HadGEM2-ES, RCP8.5) projected the frequency of deep ventilation events to be about 1 in 7.7 years by 2100 and lake surface temperatures never cooling to less than  $4 \text{ }^\circ\text{C}$  after 2050. All RCP4.5 scenarios predicted that the system would warm to the point that the entire water column is greater than the  $4 \text{ }^\circ\text{C}$  threshold (the maximum temperature of maximum density) for increasing lengths of time. All RCP8.5 scenarios predicted that the system would warm to the point that the entire water column would be greater than the  $4 \text{ }^\circ\text{C}$  threshold by the year 2060 for the HadGEM2 models and by the year 2080 for the CNRM-CM5 model; thus, the conditions required for thermobaric instability induced mixing become rare or non-existent.

The historical role of the atmosphere in the heat budget of Crater Lake has been to cool the deep waters of the lake and vent the hydrothermal heat flux to the atmosphere (we estimated the hydrothermal heat flux to be about  $1.4 \text{ W/m}^2$ , which is somewhat larger but the same order of magnitude as the previous estimate of  $1 \text{ W/m}^2$ ). The primary effects of warmer future climates on the lake are decreased frequency of episodic cooling of the hypolimnion, a transition from the lake as a heat source to a heat sink for the atmosphere, and a progressive shift in the thermal regime of Crater Lake from dimictic to warm monomictic to oligomictic. In the complete absence of deep ventilation events, the water temperature in the deep lake can increase by about  $0.39 \text{ }^\circ\text{C}$  per decade based on hydrothermal inputs alone, so this provides an upper limit for the rate of temperature increase between episodic mixing.

The disruption of deep ventilation by itself does not provide a complete picture of the potential ecological and water quality consequences of warming climate to Crater Lake. The depth, timing, and frequency of vertical water column mixing are among the most important processes in deep lakes as vertical mixing often controls the growth of algae and water clarity through redistribution of nutrients and replenishes dissolved oxygen near the lake bottom that is otherwise depleted by the decomposition of organic material raining down from above. The disruption of deep ventilation has the potential to deplete oxygen levels in the deep lake and alter benthic communities living on the lake floor. Likewise, changes in the frequency of deep ventilation would affect the vertical movement of nutrients and alter both the subsequent growth of algae during summer and the corresponding water clarity for which Crater Lake is famous. Estimating the effect of warming climate on deep water oxygen depletion and water clarity will require careful modeling studies to combine the physical mixing processes affected by the atmosphere with the multitude of factors affecting the growth of algae and corresponding water clarity.

## Acknowledgments

This modeling work was supported by the U.S. Geological Survey (USGS)-National Park Service (NPS) Water Quality Partnership Program. The long-term climatological and year-round water column temperature data collected at Crater Lake was initiated by NPS and USGS Global Change Research Programs and extensive collaboration between the NPS and the College of Oceanic and Atmospheric Sciences at Oregon State University. In particular, we thank Dr. Robert Collier, Dr. Jack Dymond, and Mr. J. Chris Moser.

## References Cited

- Abatzoglou, J.T., and Brown, T.J., 2012, A comparison of statistical downscaling methods suited for wildfire applications: *International Journal of Climatology*, doi:10.1002/joc.2312.
- Ambrosetti, W., and Barbanti, L., 1999, Deep water warming in lakes—An indicator of climatic change: *Journal of Limnology*, v. 58, p. 1–9.
- Bacon, C.R., Gardner, J.V., Mayer, L.A., Buktenica, M.W., Dartnell, P., Ramsey, D.W., and Robinson, J.E., 2002, Morphology, volcanism, and mass wasting in Crater Lake, Oregon: *Geological Society of America Bulletin*, v. 114, no. 6, p. 675–692.
- Boehrer, B., and Schultze, M., 2008, Stratification of lakes: *Reviews of Geophysics*, v. 46, RG2005, doi:10.1029/2006RG000210.
- Butcher, J.B., Nover, D., Johnson, T.E., and Clark, C.M., 2015, Sensitivity of lake thermal and mixing dynamics to climate change: *Climatic Change*, v. 129, p. 295–305, doi:10.1007/s10584-015-1326-1.
- Coats, R., Perez-Losada, J., Schladow, G., Richards, R., and Goldman, C., 2006, The warming of Lake Tahoe: *Climatic Change*, v. 76, p. 121–148.
- Crawford, G.B., and Collier, R.W., 2007, Long-term observations of deepwater renewal in Crater Lake, Oregon: *Hydrobiologia*, v. 574, p. 47–68.
- Crawford, T.M., and Duchon, C.E., 1999, An improved parameterization for estimating effective atmospheric emissivity for use in calculating daytime downwelling longwave radiation: *Journal of Applied Meteorology*, v. 38, p. 474–480.
- Diaz-Nieto, J., and Wilby, R.L., 2005, A comparison of statistical downscaling and climate change factor methods—Impacts on low flows in the River Thames, United Kingdom: *Climatic Change*, v. 69, p. 245–268.
- Dokulil, M.T., Jagsch, A., George, G.D., Anneville, O., Jankowski, T., Wahl, B., Lenhart, B., Blenckner, T., and Teubner, K., 2006, Twenty years of spatially coherent deepwater warming in lakes across Europe related to the North Atlantic Oscillation: *Limnology and Oceanography*, v. 51, p. 2,787–2,793.
- Dymond, J., Collier, R., and McManus, J., 1996, Unbalanced particle flux budgets in Crater Lake, Oregon—Implications for edge effects and sediment focusing in lakes: *Limnology and Oceanography*, v. 41, no. 4, p. 732–742.
- Elo, A., Huttula, T., Peltonen, A., and Virta, J., 1998, The effects of climate change on the temperature conditions of lakes: *Boreal Environmental Research*, v. 3, p. 137–150.
- Environmental and Water Resources Institute, 2005, The ASCE Standardized Reference Evapotranspiration Equation—Final report prepared by the Task Committee on Standardization of Reference Evapotranspiration: Reston, Virginia, Environmental and Water Resources Institute of the American Society of Civil Engineers, 59 p.
- Groeger, A.W., 2007, Nutrient limitation in Crater Lake, Oregon: *Hydrobiologia*, v. 574, p. 205–216.
- Hampton, S.E., Izmet'eva, L.R., Moore, M.V., Katz, S.L., Dennis, B., and Silow, E.A., 2008, Sixty years of environmental change in the world's largest freshwater lake—Lake Baikal, Siberia: *Global Change Biology*, v. 14, p. 1,947–1,958, doi:10.1111/j.1365-2486.2008.01616.x.
- Hostetler, S.W., and Giorgi, F., 1995, Effects of a 2XCO<sub>2</sub> climate on two large lake systems: Pyramid Lake, Nevada, and Yellowstone Lake, Wyoming: *Global and Planetary Change*, v. 10, p. 43–54.
- Hostetler, S.W., and Small, E.E., 1999, Response of North American freshwater lakes to simulated future climates: *Journal of the American Water Resources Association*, v. 35, p. 1,625–1,637.
- Imerito, A., 2014, Dynamic Reservoir Simulation Model DYRESM v4—v4.0 science manual: Perth, University of Western Australia, Centre for Water Research, 42 p.
- Jassby, A., and Powell, T., 1975, Vertical patterns of eddy diffusion during stratification in Castle Lake, California: *Limnology and Oceanography*, v. 20, p. 530–543.

- Kullenberg, G., 1976, On vertical mixing and the energy transfer from the wind to the water: *Tellus B*, v. 28, no. 2, p. 159–165.
- Livingstone, D., 1997, An example of the simultaneous occurrence of climate-driven “sawtooth” deep-water warming/cooling episodes in several Swiss lakes: *Verhandlungen des Internationalen Verein Limnologie*, v. 26, p. 822–828.
- Livingstone, D., 2003, Impact of secular climate change on the thermal structure of a large temperate central European lake: *Climatic Change*, v. 57, p. 205–255.
- Martin, J.L., and McCutcheon, S.C., 1998, *Hydrodynamics and transport for water quality modeling*: Boca Raton, Florida, CRC Press, 816 p.
- Marty, Ch., Philipona, R., Fröhlich, C., and Ohmura, A., 2002, Altitude dependence of surface radiation fluxes and cloud forcing in the alps—Results from the alpine surface radiation budget network: *Theoretical and Applied Climatology*, v. 72, p. 137–155.
- McManus, J., Collier, R.W., Chen, C.A., and Dymond, J., 1992, Physical properties of Crater Lake, Oregon—A method for the determination of a conductivity and temperature-dependent expression for salinity: *Limnology and Oceanography*, v. 37, p. 41–53.
- McManus, J., Collier, R.W., and Dymond, J., 1993, Mixing processes in Crater Lake, Oregon: *Journal of Geophysical Research*, v. 98, p. 18,295–18,307.
- Mellor, G.L., 1989, Retrospect on oceanic boundary layer modeling and second moment closure, *in* Muller, P., and Henderson, D., eds., *The parameterization of small-scale processes: Proceedings of the 5th Aha Huliko’a Hawaiian Winter Workshop*, January 1989: Honolulu, University of Hawaii at Manoa, p. 251–272.
- Met Office, 2014, Met Office climate prediction model—HadGEM2 family: Met Office Web site, accessed December 24, 2015, at <http://www.metoffice.gov.uk/research/modelling-systems/unified-model/climate-models/hadgem2>.
- Minville, M., Brissette, F., and Leconte, R., 2008, Uncertainty of the impact of climate change on the hydrology of a Nordic watershed: *Journal of Hydrology*, v. 358, p. 70–83.
- Munk, W.H., and Anderson, E.R., 1948, Notes on a theory of the thermocline: *Journal of Marine Research*, v. 7, p. 276–295.
- National Atmospheric and Space Administration, 2015, Ocean in motion—Ekman Transport—Background: National Atmospheric and Space Administration Web site, accessed December 24, 2015, at <http://oceanmotion.org/html/background/ocean-in-motion.htm>.
- National Centre of Meteorological Research, 2014, CNRM-CM5—Description: National Centre of Meteorological Research Web site, accessed December 24, 2015, at <http://www.cnrm-game.fr/spip.php?article126&lang=en>.
- Pacanowski, R.C., and Philander, S.G., 1981, Parameterization of vertical mixing in numerical models of tropical oceans: *Journal of Physical Oceanography*, v. 11, p. 1,443–1,451.
- Panofsky, H.A., and Brier, G.W., 1968, *Some applications of statistics to meteorology*: The Pennsylvania State University, College of Earth and Mineral Sciences, 224 p.
- Peeters, F., Livingstone, D.M., Goudsmit, G., Kipfer, R., and Forster, R., 2002, Modeling 50 years of historical temperature profiles in a large central European lake: *Limnology and Oceanography*: v. 47, p. 186–197.
- Peeters, F., Straile, D., Lorke, A., and Livingstone, D., 2007, Earlier onset of the spring phytoplankton bloom in lakes of the temperate zone in a warmer climate: *Global Change Biology*, v. 13, p. 1,898–1,909, doi:10.1111/j.1365-2486.2007.01412.x.
- Perroud, M., and Goyette, S., 2010, Impact of warmer climate on Lake Geneva water-temperature profiles: *Boreal Environment Research*, v. 15, p. 255–278.
- Piccolroaz, S., 2013, Deep ventilation in Lake Baikal—A simplified model for a complex natural phenomenon: Italy, University of Trento, Ph.D. thesis, 172 p., accessed February 2014 at <http://eprints-phd.biblio.unitn.it/1012/>.
- Piccolroaz, S., and Toffolon, M., 2013, Deep water renewal in Lake Baikal—A model for long-term analyses: *Journal of Geophysical Research*, v. 118, p. 6,717–6,733.

- Piccolroaz, S., Toffolon, M., and Majone, B., 2013, A simple lumped model to convert air temperature into surface water temperature in lakes: *Hydrology and Earth System Sciences*, v. 17, p. 3,323–3,338, doi:10.5194/hess-17-3323-2013.
- Piccolroaz, S., Toffolon, M., and Majone, B., 2015, The role of stratification on lakes' thermal response—The case of Lake Superior: *Water Resources Research*, v. 51, p. 7,878–7,894, doi:10.1002/2014WR016555.
- Powell, T., and Jassby, A., 1974, The estimation of vertical eddy diffusivities below the thermocline in lakes: *Water Resources Research*, v. 10, p. 191–198.
- Ravens, T.M., Kocsis, O., and Wüest, A., 2000, Small-scale turbulence and vertical mixing in Lake Baikal: *Limnology and Oceanography*, v. 45, p. 159–173.
- Riahi, K., Rao, S., Krey, V., Cho, C., Chirkov, V., Fischer, G., Kindermann, G., Nakicenovic, N., and Rafaj, P., 2011, RCP8.5—A scenario of comparatively high greenhouse gas emissions: *Climatic Change*, v. 109, p. 33–57, doi:10.1007/s10584-011-0149-y.
- Robertson, D.M., and Ragotzkie, R.A., 1990, Changes in the thermal structure of moderate to large sized lakes in response to changes in air temperature: *Aquatic Sciences*, v. 52, p. 360–380.
- Ruckstuhl, C., Philipona, R., Morland, J., and Ohmura, A., 2007, Observed relationship between surface specific humidity, integrated water vapor, and longwave downward radiation at different altitudes: *Journal of Geophysical Research*, v. 112, p. D03302, doi:10.1029/2006JD007850.
- Rupp, D.E., Abatzoglou, J.T., Hegewisch, K.C., and Mote, P.W., 2013, Evaluation of CMIP5 20th century climate simulations for the Pacific Northwest USA: *Journal of Geophysical Research*, v. 118, p. 10,884–10,906, doi:10.1002/jgrd.50843.
- Simpson, H.J., 1970, Tritium in Crater Lake, Oregon: *Journal of Geophysical Research*, v. 75, p. 5,195–5,207.
- Sweers, H.E., 1970, Vertical diffusivity coefficient in a thermocline: *Limnology and Oceanography*, v. 15, p. 273–280.
- Swinbank, W.C., 1963, Long-wave radiation from clear skies: *Quarterly Journal of the Royal Meteorological Society*, v. 89, p. 339–348.
- Taylor, K.E., Stouffer, R.J., and Meehl, G.A., 2012, An Overview of CMIP5 and the experiment design: *Bulletin of the American Meteorological Society*, v. 93, p. 485–498, doi:10.1175/BAMS-D-11-00094.1.
- Thomson, A.M., Calvin, K.V., Smith, S.J., Kyle, G.P., Volke, A., Patel, P., Delgado-Arias, S., Bond-Lamberty, B., Wise, M.A., Clarke, L.E., and Edmonds, J.A., 2011, RCP4.5—A pathway for stabilization of radiative forcing by 2100: *Climatic Change*, v. 109, p. 77–94, doi:10.1007/s10584-011-0151-4.
- Toffolon, M., Piccolroaz, S., Majone, B., Soja, A.M., Peeters, F., Schmid, M., and Wüest, A., 2014, Prediction of surface water temperature from air temperature in lakes with different morphology: *Limnology and Oceanography*, v. 59, no. 6, p. 2,185–2,202, doi:10.4319/lo.2014.59.6.2185.
- Tucker, W.A., and Green, A.W., 1977, A time-dependent model of the lake-averaged, vertical temperature distribution of lakes: *Limnology and Oceanography*, v. 22, p. 687–699.
- Weiss, R.F., 1992, Rates and variability of deep water renewal and biological production in deep temperate lakes—Lake Baikal and Crater Lake [abs]: *Eos, Transactions American Geophysical Union*, v. 73, iss. 43, p. 198.
- Wüest, A.T., Ravens, M., Granin, N.G., Kocsis, O., Schurter, M., and Sturm, M., 2005, Cold intrusions in Lake Baikal—Direct observational evidence for deep water renewal: *Limnology and Oceanography*, v. 50, p. 184–196.
- Yang, K., He, J., Tang, W., Qin, J., and Cheng, C.C.K., 2010, On downward shortwave and longwave radiations over high altitude regions—Observation and modeling on the Tibetan Plateau: *Agricultural and Forest Meteorology*, v. 150, p. 38–46, doi:10.1016/j.agrformet.2009.08.004.



Publishing support provided by the U.S. Geological Survey  
Science Publishing Network, Tacoma Publishing Service Center

For more information concerning the research in this report, contact the  
Director, Oregon Water Science Center  
U.S. Geological Survey  
2130 SW 5th Avenue  
Portland, Oregon 97201  
<http://or.water.usgs.gov>

